

# From Zero-Shot to Few-Shot Learning: A Step of Embedding-Aware Generative Models

Liangjun Feng, Jiancheng Zhao, Chunhui Zhao, *Senior Member, IEEE*

**Abstract**—Embedding-aware generative model (EAGM) addresses the data insufficiency problem for zero-shot learning (ZSL) by constructing a generator between semantic and visual embedding spaces. Thanks to the predefined benchmark and protocols, the number of proposed EAGMs for ZSL is increasing rapidly. We argue that it is time to take a step back and reconsider the embedding-aware generative paradigm. The purpose of this paper is three-fold. First, given the fact that the current embedding features in benchmark datasets are somehow out-of-date, we improve the performance of EAGMs for ZSL remarkably with embarrassingly simple modifications on the embedding features. This is an important contribution, since the results reveal that the embedding of EAGMs deserves more attention. Second, we compare and analyze a significant number of EAGMs in depth. Based on five benchmark datasets, we update the state-of-the-art results for ZSL and give a strong baseline for few-shot learning (FSL), including the classic unseen-class few-shot learning (UFSL) and the more challenging seen-class few-shot learning (SFSL). Finally, a comprehensive generative model repository, namely, generative any-shot learning (GASL) repository, is provided, which contains the models, features, parameters, and settings of EAGMs for ZSL and FSL. Any results in this paper can be readily reproduced with only one command line based on GASL.

**Index Terms**—Zero-shot learning, few-shot learning, generative model, semantic embedding, feature embedding.

## 1 INTRODUCTION

SUPPORTED by large-scale annotated datasets [1], [2], intelligent models, *e.g.*, convolutional neural networks (CNNs) [3], [4], [5], [6] and transformers [7], [8], have presented encouraging breakthroughs in visual recognition in the last decade. From 2012 to 2022, the top-5 accuracy of image recognition task on ImageNet1k has rapidly increased from 83% to 98% [9], [10]. However, due to the long-tailed distribution of categories, instance collection for rare objects in the standard supervised learning is practically expensive and time-consuming [10], [11], [12]. With few training exemplars or category-unbalanced dataset, popular intelligent models usually fail to present the state-of-the-art results. [13], [14]

To address the challenge, zero-shot learning (ZSL) [15], [16] is designed to train a model capable of recognizing unseen objects based on the dataset of seen objects. In comparison with traditional supervised learning task, there are unique techniques for ZSL to achieve knowledge transfer from seen classes to unseen classes [17], [18], [19], [20]. On the one hand, some auxiliary information, *e.g.*, attribute or textual description of class label, is used in ZSL to bridge the class gap between seen and unseen classes. This technique, known as *semantic embedding* [21], [22], [23], [24], allows to identify a new object by having only a description of it. The semantic embedding can be obtained by manual annotation or individual representation models. For example, eighty-five manually annotated attributes are used in the bench-

mark Animals with Attributes (AWA) dataset [15] to describe fifty kinds of animals, and 1,024-dimensional features extracted by the character-based CNN-RNN model [25] are used in the benchmark Oxford Flowers (FLO) dataset [26] to describe 102 kinds of flowers. On the other hand, empirical studies [27], [28], [29], [30] have indicated that replacing the original images with the features from a pretrained CNN, known as *visual embedding*, makes ZSL more effective for recognition task. Currently, the visual embeddings used in benchmark datasets are 2,048-dim top-layer pooling units of ResNet101 [13], which is pretrained on ImageNet 1K [1] and not finetuned. With the well-designed semantic and visual embedding, models of ZSL [31], [32], [33], [34] learn from seen objects and predict for unseen objects. Particularly, when all classes are allowed at test phase, the problem is defined as generalized zero-shot learning (GZSL) [27], [28], [35], [36], [37]. In comparison with the conventional ZSL, GZSL removes the unreasonable restriction that test data only come from unseen classes and hence is more practical.

Due to the importance of ZSL and GZSL, the number of new ZSL methods proposed every year has been increasing rapidly. These methods can be categorized into various paradigms, such as probability-based methods [15], [17], [38], compatibility-based methods [18], [39], [40], [41], [42], image-aware generative models (IAGMs) [43], [44], [45], [46], [47], and *embedding-aware generative models* (EAGMs) [48], [49], [50], [51], [52], [53], [54], [55]. The probability-based methods, *e.g.*, DAP [15] and TIZSL [38], learn a number of probabilistic classifiers for attributes and combine the probability outputs to make predictions. The compatibility-based methods, *e.g.*, DeVISE [41] and ESZSL [18], learn a compatibility function between the semantic and visual features, which gives ranking scores for classification. As for generative models, they train conditional generators,

- Liangjun Feng, Jiancheng Zhao and Chunhui Zhao are with the State Key Laboratory of Industrial Control Technology, College of Control Science and Engineering, Zhejiang University, Hangzhou 310027, China.
- E-mail: chhzhao@zju.edu.cn, liangjunfeng@zju.edu.cn, zhao-jiancheng@zju.edu.cn.
- Corresponding author: Chunhui Zhao.

Manuscript received xxx xx, xxxx; revised xxx xx, xxxx.

*e.g.*, generative adversarial networks (GANs) [56], [57] and variational autoencoders (VAEs) [58], [59], based on the semantic embedding to synthesize virtual exemplars for unseen classes. Specifically, IAGMs aim to synthesize original images, while EAGMs aim to synthesize visual features. In comparison with other paradigms, EAGMs address the essential data insufficiency problem and enjoy both semantic embedding and visual embedding [48], [50]. Hence, EAGMs have presented state-of-the-art results for ZSL and GZSL and have become more and more popular in recent years [60], [61], [62], [63], [64]. In this paper, we focus on EAGMs.

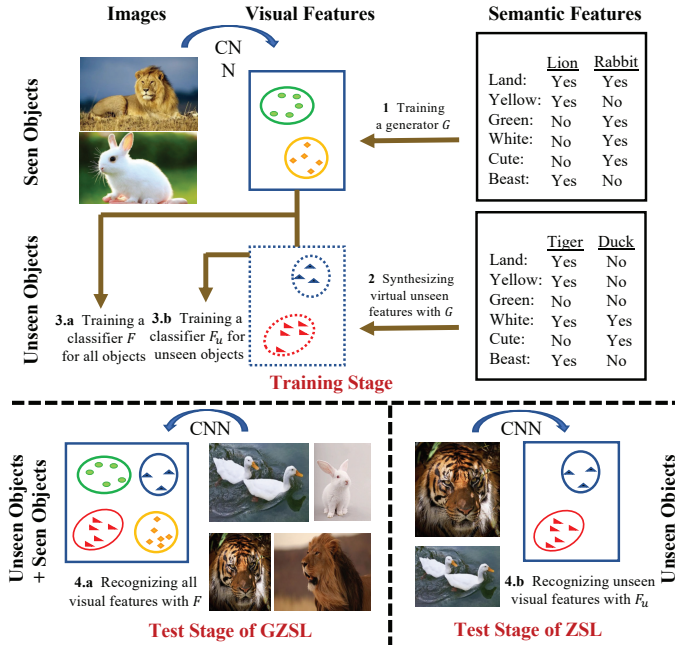


Fig. 1. A schematic diagram of EAGM for ZSL and GZSL. The feature generator  $G$  is constructed between the semantic and visual embedding spaces. Order of GZSL: 1-2-3.a-4.a; Order of ZSL: 1-2-3.b-4.b.

Particularly, we give an interesting observation that the usage of benchmarked embedding features has both pros and cons for EAGMs. For clarification, we visualize EAGM for ZSL and GZSL in Figure 1. For GZSL, the paradigm of EAGM is applied as 1-2-3.a-4.a; For ZSL, EAGM is applied as 1-2-3.b-4.b. As shown, the generator  $G$  is assigned to learn the mapping from semantic embedding space to visual embedding space. On the one hand, the embedding features contributed by Xian *et al.* [27], [28] indeed provide a fair experimental setting. Based on the benchmark, numerous regularizations, *e.g.*, cycle loss [65], [66], and implementations, *e.g.*, Wasserstein GAN (WGAN) [48], [56], are proposed for  $G$  to enhance its generation capability. On the other hand, we argue that the research of EAGMs on ZSL and GZSL should not be limited to the generator  $G$ . The embedding features deserve more attention. Essentially, ZSL and GZSL are classification tasks whose performance are upper bounded by the features. A perfect generator would make few effects with poor embedding features. In the previous works of Xian *et al.* [67] and Narayan *et al.* [68], the original ResNet visual features in benchmark datasets were replaced with finetuned ResNet visual features, resulting in a significant performance improvement. Before finetuning,

f-VAEGAN-D2 achieved a harmonic mean of 64.6% on FLO for GZSL, while the number increased to 75.1% afterward. The simple but effective trial reveals that the enhancement for embedding features is promising. However, Xian *et al.* [67] and Narayan *et al.* [68] did not discuss or analyze this phenomenon. Here, we take a further step to explore the effects of embeddings for EAGMs in depth, including the visual embedding and semantic embedding.

Besides, EAGMs can be readily applied for few-shot learning (FSL) tasks [70], [71], [72], [73], [74], [75]. In comparison with ZSL, FSL allows a few samples per unseen class for model training. Sometimes, the scenario where only a few samples per seen class are used for model training is also called few-shot learning [76]. To avoid misunderstanding, we name the former scenario as unseen-class few-shot learning (UFSL) and the latter scenario as seen-class few-shot learning (SFSL). Like GZSL, the more practical generalized unseen-class few-shot learning (GUFSL) and generalized seen-class few-shot learning (GSFSL) can be obtained from UFSL and SFSL respectively by making all classes available for test. The mathematical formulations for any-shot learning, *i.e.*, ZSL, GZSL, UFSL, GUFSL, SFSL, and GSFSL, would be given in the preliminary section for clarification. Generally, the challenge of FSL is that directly training the model in the case of a few samples results in serious overfitting and unsatisfactory performance [77], [78]. Because EAGMs are designed to synthesize virtual exemplars for objects, they could treat FSL as a data insufficiency problem and address it like in ZSL. Some EAGMs, *e.g.*, CADA-VAE [79] and TGG [80], have already been applied for FSL and obtained superior performance. However, distinguished from the comparison in ZSL, we argue that the comparison of EAGMs in FSL has no agreed upon protocols. Various experimental settings may be used by different methods, leading to unfair comparisons. For example, the few samples used in model training determine the learning quality of EAGMs for FSL. Difference in the chosen samples would affect the comparison results. Besides, as shown in the FSL experiments presented by Zhang *et al.* [80] and Schonfeld *et al.* [79], only one or two methods were used for comparison, which seems insufficient. This phenomenon reveals the lack of baseline results for EAGMs in FSL. It is desired to obtain a unified experimental setting and baseline for FSL like those for ZSL.

**Contributions:** In this paper, we perform comprehensive experiments to explore the potential of embedding-aware generative paradigms in depth from the perspective of embeddings and tasks, which are valuable facing the widespread data insufficiency problem. We emphasize the importance of improving embeddings for EAGMs, including the semantic embedding and visual embedding, as satisfactory results can hardly be obtained from a generator with coarse-grained features. We argue that the current embeddings used in benchmark datasets for ZSL are somehow out-of-date, which are based on the methods proposed in 2015 [13] and 2016 [25]. With the recent advances in deep learning, we update the state-of-the-art results for ZSL and GZSL using embarrassingly simple modifications on the embeddings. Moreover, considering FSL is also an important application of EAGMs, the fact is given that there is actually no agreed upon protocols for the comparison of EAGMs

TABLE 1  
Summary of Six Tasks for EAGMs

NO.	Task	Full Name	Type	# Methods	Training $\rightarrow$ Test		Challenge
					Training set	Test set	
1	ZSL	Zero-Shot Learning	Z	Numerous	$\mathcal{X}_s \cup \mathcal{Y}_s \cup \mathcal{A}$	$\mathcal{X}_u$	Middle
2	GZSL	Generalized Zero-Shot Learning	Z	Numerous	$\mathcal{X}_s^{tr} \cup \mathcal{Y}_s^{tr} \cup \mathcal{A}$	$\mathcal{X}_u \cup \mathcal{X}_s^{te}$	
3	UFSL	Unseen-class Few-Shot Learning	F	Some	$\mathcal{X}_s \cup \mathcal{Y}_s \cup \mathcal{X}_u^{tr-f} \cup \mathcal{Y}_u^{tr-f} \cup \mathcal{A}$	$\mathcal{X}_u^{te}$	Low
4	GUFSL	Generalized Unseen-class Few-Shot Learning	F	Some	$\mathcal{X}_s^{tr} \cup \mathcal{Y}_s^{tr} \cup \mathcal{X}_u^{tr-f} \cup \mathcal{Y}_u^{tr-f} \cup \mathcal{A}$	$\mathcal{X}_u^{te} \cup \mathcal{X}_s^{te}$	
5	SFSL	Seen-class Few-Shot Learning	Z+F	A Few	$\mathcal{X}_s^{tr-f} \cup \mathcal{Y}_s^{tr-f} \cup \mathcal{A}$	$\mathcal{X}_u$	High
6	GSFSL	Generalized Seen-class Few-Shot Learning	Z+F	A Few	$\mathcal{X}_s^{tr-f} \cup \mathcal{Y}_s^{tr-f} \cup \mathcal{A}$	$\mathcal{X}_u \cup \mathcal{X}_s^{te}$	

Note: "Z" denotes the task is a kind of zero-shot learning and "F" denotes the task is a kind of few-shot learning.

in FSL. Based on five benchmark datasets, we reproduce a significant number of EAGMs and present strong baseline results for FSL, including UFSL, GUFSL, SFSL, and GSFSL. With these works, newly proposed EAGMs can be sufficiently evaluated on FSL. Finally, we make our work a publicly available repository, namely generative any-shot learning (GASL) repository, which contains the models, features, parameters, and settings of EAGMs for ZSL and FSL. Any results in this paper can be readily reproduced with only one command line based on GASL. Therefore, we argue that our work plays an important role in pushing EAGMs a step forward from zero-shot learning to few-shot learning or any-shot learning.

**Organization:** This paper contains seven sections. Section 2 gives some preliminary works, including the basic notations and formulations. Section 3 reviews related works on zero-shot learning and embedding-aware generative models. Section 4 focuses on the analysis of reproduced models. Section 5 shows our modifications on the visual embedding and semantic embedding. Section 6 presents ZSL and FSL experiments for EAGMs based on benchmark datasets. A discussion on the trends for future research, along with our conclusions, is presented in Section 7.

## 2 PRELIMINARY

### 2.1 Basic Notations

For visual recognition, we have a set of seen classes,  $\mathcal{Y}_s = \{1, \dots, p\}$ , and a set of unseen classes,  $\mathcal{Y}_u = \{p+1, \dots, p+q\}$ . The two sets are disjoint, *i.e.*,  $\mathcal{Y}_s \cap \mathcal{Y}_u = \emptyset$ ,  $p$  is the number of seen classes, and  $q$  is the number of unseen classes. In comparison, seen classes have sufficient samples for model training, while unseen classes have no or a few samples for model training. Suppose that a dataset of seen classes is  $\mathcal{D}_s = \{(x_s^{(i)}, y_s^{(i)}, a_s^{(i)})\}$ ,  $i = 1, \dots, N_s$ , where  $x_s^{(i)} \in \mathcal{X}_s$  is a visual feature with a corresponding class label  $y_s^{(i)} \in \mathcal{Y}_s$  and a semantic description  $a_s^{(i)} \in \mathcal{A}_s$ . Similarly, a dataset of unseen classes is  $\mathcal{D}_u = \{(x_u^{(i)}, y_u^{(i)}, a_u^{(i)})\}$ ,  $i = 1, \dots, N_u$ , where  $x_u^{(i)} \in \mathcal{X}_u$ ,  $y_u^{(i)} \in \mathcal{Y}_u$ , and  $a_u^{(i)} \in \mathcal{A}_u$ . We also use  $x_{s_i}, y_{s_i}, a_{s_i}$  and  $x_{u_i}, y_{u_i}, a_{u_i}$  to denote the items of the  $i$ -th seen and unseen class, respectively.

Note that the visual feature  $x$  is an embedding of the image,  $v$ , *i.e.*,  $x = E_x(v)$ , where  $E_x$  is the visual embedding function, *e.g.*, the pretrained CNN, for  $v$ . The semantic feature  $a$  is an embedding of the class label,  $y$ , *i.e.*,  $a = E_a(t)$ , where  $t$  is the attribute or textual description of  $y$  and  $E_a$  is the semantic embedding function, *e.g.*, the character-based CNN-RNN [25], for  $t$ . All samples in class  $y$  enjoy the same

$a$ . In comparison with conventional supervised learning tasks, the semantic information  $a$  is introduced here as the prior knowledge of each class for model designing.

### 2.2 Problem Formulations

In this paper, six scenarios are considered for EAGMs, including ZSL, GZSL, UFSL, GUFSL, SFSL, and GSFSL. Based on the defined notations, these tasks are formulated and explained as follows.

- 1) ZSL: Zero-shot learning aims to train a discriminant function based on the seen dataset and all the semantic descriptions. The evaluation of the discriminant function is performed on the unseen classes. Hence, the paradigm of ZSL is  $\mathcal{X}_s \cup \mathcal{Y}_s \cup \mathcal{A} \rightarrow \mathcal{X}_u$ .
- 2) GZSL: Generalized zero-shot learning is an extension of ZSL. Both seen and unseen classes are allowed for test. Hence, the paradigm of GZSL is  $\mathcal{X}_s^{tr} \cup \mathcal{Y}_s^{tr} \cup \mathcal{A} \rightarrow \mathcal{X}_u \cup \mathcal{X}_s^{te}$ , where  $\mathcal{X}_s^{tr} \cup \mathcal{Y}_s^{tr}$  and  $\mathcal{X}_s^{te}$  denote the training sample pairs and test samples of seen classes, respectively.
- 3) UFSL: Unseen-class few shot learning trains a discriminant function with the seen dataset and a few unseen sample pairs. The evaluation is performed on the unseen classes. Hence, the paradigm of UFSL is  $\mathcal{X}_s \cup \mathcal{Y}_s \cup \mathcal{X}_u^{tr-f} \cup \mathcal{Y}_u^{tr-f} \cup \mathcal{A} \rightarrow \mathcal{X}_u^{te}$ , where  $\mathcal{X}_u^{tr-f} \cup \mathcal{Y}_u^{tr-f}$  denotes a few training sample pairs of unseen classes.
- 4) GUFSL: Generalized unseen-class few-shot learning is an extension of UFSL. Both seen and unseen classes are allowed for test. Hence, the paradigm of GUFSL is  $\mathcal{X}_s^{tr} \cup \mathcal{Y}_s^{tr} \cup \mathcal{X}_u^{tr-f} \cup \mathcal{Y}_u^{tr-f} \cup \mathcal{A} \rightarrow \mathcal{X}_u^{te} \cup \mathcal{X}_s^{te}$ .
- 5) SFSL: Seen-class few-shot learning trains a discriminant function with only a few seen sample pairs. The evaluation is performed on the unseen classes. Hence, the paradigm of SFSL is  $\mathcal{X}_s^{tr-f} \cup \mathcal{Y}_s^{tr-f} \cup \mathcal{A} \rightarrow \mathcal{X}_u$ , where  $\mathcal{X}_s^{tr-f} \cup \mathcal{Y}_s^{tr-f}$  is a few training sample pairs of seen classes.
- 6) GSFSL: Generalized seen-class few-shot learning is an extension of SFSL. Both seen and unseen classes are allowed for test. Hence, the paradigm of GSFSL is  $\mathcal{X}_s^{tr-f} \cup \mathcal{Y}_s^{tr-f} \cup \mathcal{A} \rightarrow \mathcal{X}_u \cup \mathcal{X}_s^{te}$ .

For clarification, the six tasks are listed and compared in Table 1. Generally, SFSL and GSFSL can be treated as hybrid tasks of ZSL and FSL and are more challenging than others, since they have only a few seen sample pairs for model training. However, only a few EAGM-based methods [76]

have been proposed for SFSL and GSFSL. Most of EAGM-based methods [50], [51], [52], [53], [54], [55], [79], [80] are designed for ZSL and GZSL, and some of them [79], [80] are used for UFSL and GUFSL.

## 2.3 Formulations of EAGMs

### 2.3.1 Formulation of EAGMs for ZSL

Generally, EAGMs first train a generator,  $G$ , based on seen classes by:

$$\frac{1}{N_s} \sum_{n=1}^{N_s} \mathcal{L}_g(x_s, y_s, a; W_g) + \Omega(W_g), \quad (1)$$

where  $\mathcal{L}_g$  is the loss function of  $G$ ,  $\Omega$  is the regularization term, and  $W_g$  is the model parameter.

Based on the well-trained  $G$ , a classifier of unseen classes,  $F_u$ , can be obtained for ZSL by:

$$\frac{1}{\tilde{N}_u} \sum_{n=1}^{\tilde{N}_u} \mathcal{L}_{f_u}(\tilde{x}_u, \tilde{y}_u, a_u; W_{f_u}), \quad (2)$$

$$\tilde{x}_u = G(a_u, z),$$

where  $\mathcal{L}_{f_u}$  is the loss function of  $F_u$ ,  $\tilde{x}_u$  and  $\tilde{y}_u$  are generated sample pairs for unseen classes,  $\tilde{N}_u$  is the number of generated unseen samples,  $W_{f_u}$  is the model parameter, and  $z \sim \mathcal{N}(0, 1)$  is the Gaussian noise. At the test stage of ZSL, the classification for unseen classes can then be readily performed by  $F_u$ .

For GZSL, a classifier for all classes,  $F$ , is obtained by:

$$\frac{1}{N_s + \tilde{N}_u} \sum_{n=1}^{N_s + \tilde{N}_u} \mathcal{L}_f(x_s, y_s, \tilde{x}_u, \tilde{y}_u, a; W_f), \quad (3)$$

where  $\mathcal{L}_f$  is the loss function of  $F$  and  $W_f$  is the parameter of  $F$ .

### 2.3.2 Formulation of EAGMs for FSL

In UFSL and GUFSL, the generator of all classes,  $G$ , can be directly trained as:

$$\frac{1}{N_s + qN} \sum_{n=1}^{N_s + qN} \mathcal{L}_g(x_s, y_s, x_u, y_u, a; W_g) + \Omega(W_g), \quad (4)$$

where  $q$  is the number of unseen classes and  $N$  is the number of provided samples for each unseen classes in the training stage.

For UFSL, a classifier of unseen classes,  $F_u$ , can be trained by:

$$\frac{1}{qN + \tilde{N}_u} \sum_{n=1}^{qN + \tilde{N}_u} \mathcal{L}_{f_u}(x_u, y_u, \tilde{x}_u, \tilde{y}_u, a_u; W_{f_u}), \quad (5)$$

and for GUFSL, a classifier of all classes,  $F$ , is obtained by:

$$\frac{1}{N_s + qN + \tilde{N}_u} \sum_{n=1}^{N_s + qN + \tilde{N}_u} \mathcal{L}_f(x_s, y_s, x_u, y_u, \tilde{x}_u, \tilde{y}_u, a; W_f), \quad (6)$$

where the real samples of all classes and virtual unseen samples are used in the training stage of  $F$  for the final classification.

Besides, the formulations of zero-shot learning are applicable for SFSL and GSFSL, since SFSL and GSFSL enjoy similar data splits as ZSL and GZSL.

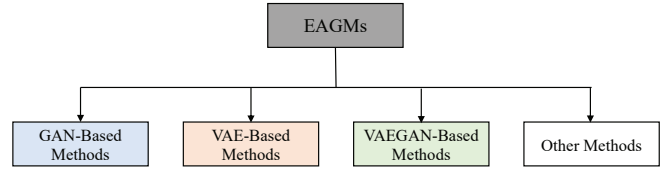


Fig. 2. A generative algorithm-based classification for popular embedding-aware generative models.

## 3 RELATED WORKS

### 3.1 Review and Evaluation of ZSL and GZSL

From the seminal paper of Lampert *et al.* [15], more and more works have been proposed for ZSL and GZSL. There are a few attempts have been made for literature review and method evaluation.

#### 3.1.1 Review and Evaluation of ZSL

At the early stage of ZSL, Song *et al.* [81] reviewed about thirty methods of ZSL and categorized them into three groups based on how the feature embedding and the semantic embedding were related. The three groups include one-order transformation models, two-order transformation models, and high-order transformation models. Also, considering the importance of semantic information for ZSL, Chen *et al.* [82] provided a survey in the perspective of external knowledge. Four types of knowledge sources, *i.e.*, text, attribute, knowledge, and rule, were summarized, and three paradigms, *i.e.*, mapping function, generative model, and graph neural network, were emphasized for their promising performance on ZSL. However, this survey did not compare and analyze the performance of different patterns. Fu *et al.* [83] reported the recent advances in ZSL from the perspective of semantic representation, model, dataset, and problem. Specifically, the semantic spaces were categorized based on whether they were attribute space or not. The models in ZSL were summarized in a unified “embedding model and recognition model in embedding space” framework. Fifteen datasets and two problems including the projection domain shift problem and the hubness problem of ZSL were listed and discussed. From the four perspectives, although the definition and paradigm of ZSL can be introduced in detail, the performance comparison and state-of-the-art results were ignored. Similarly, in the work of Wang *et al.* [84], the settings, methods, and applications of ZSL were comprehensively reviewed. Based on the data utilized in model optimization, zero-shot learning methods were classified into three learning settings, including the class-inductive instance-inductive setting, class-transductive instance-inductive setting, and class-transductive instance-transductive setting. According to the recognition styles for final classification, the methods were categorized into the classifier based methods and the instance-based methods. Representative models under each category and their applications were also introduced. These works pay more attention on the setting and category of ZSL in stead of model techniques and do not analyze the generalized zero-shot learning task in depth.

TABLE 2  
Comparison of Mentioned Reviews and Evaluations

NO. Paper	Task						EAGMs		Embedding		Sources			
	ZSL	GZSL	UFSL	GUFSL	SFSL	GSFSL	Discussion	Experiments	Discussion	Experiments	Data/Feat.	Param.	Split	Code
1 Song <i>et al.</i> [81]	✓	✗	✗	✗	✗	✗	✗	✗	✓	✗	✗	✗	✗	✗
2 Chen <i>et al.</i> [82]	✓	✗	✗	✗	✗	✗	✗	✗	✓	✗	✗	✗	✗	✗
3 Fu <i>et al.</i> [83]	✓	✗	✗	✗	✗	✗	✗	✗	✓	✗	✗	✗	✗	✗
4 Wang <i>et al.</i> [84]	✓	✗	✗	✗	✗	✗	✓	✗	✓	✗	✗	✗	✗	✗
5 Xian <i>et al.</i> [28]	✓	✓	✗	✗	✗	✗	✗	✗	✓	✓	✓	✗	✓	✗
6 Pourpanah <i>et al.</i> [85]	✓	✓	✗	✗	✗	✗	✓	✗	✓	✗	✗	✗	✗	✗
7 Ours	✓	✓	✓	✓	✓	✓	✓	✓	✓	✓	✓	✓	✓	✓

### 3.1.2 Review and Evaluation of GZSL

Xian *et al.* [28] made a comprehensive evaluation of sixteen conventional ZSL models on the GZSL task, which revealed that conventional ZSL models suffered from serious bias problem and showed degraded performance in GZSL. Meanwhile, Xian *et al.* [28] provided a unified evaluation protocol and embedding features for GZSL, which contributed a lot to transfer the research hotspot from the conventional ZSL to the more practical GZSL. However, the evaluation was still limited to the conventional ZSL models, some new paradigms, *e.g.*, generative models, were not considered for GZSL. Pourpanah *et al.* [85] made a comprehensive review for generalized zero-shot learning methods. More than sixty GZSL models were compared in three groups. The first group was the embedding-based methods, which learned a projection function to associate the low-level visual features of seen classes with their corresponding semantic vectors. The second group was the generative-based methods, which learned a model to generate exemplars for unseen classes based on the seen set. The third group was the transductive-based methods, which used unlabeled unseen samples for model training. Although numerous GZSL methods were compared in this review, the results used were directly referred from their papers. The different experimental settings may affect the comparison and conclusion.

For clarification, we summarize the mentioned reviews and evaluations in Table 2, where the work of this paper is also listed for comparison. It can be observed that our work takes more tasks of EAGMs into consideration, and pays more attentions on the effects of embeddings on EAGMs. Besides, there have been some reviews, surveys, and evaluations for transfer learning [86], [87], [88], [89], [90] and few-shot learning [91], [92], [93], [94], [95] published in recent years. Because these works do not cover the topic of embedding-aware generative models, zero-shot learning, and generalized zero-shot learning with sufficient depth, we do not discuss them in the current work.

## 3.2 Embedding-Aware Generative Models

Embedding-aware generative models synthesize virtual visual features based on semantic descriptions, which tackle the insufficient data problem for ZSL and FSL. Thanks to the superior performance and efficient training process, EAGMs have attracted more and more attentions. Generally, an ideal feature generator is required to satisfy three conditions: (1) The generated virtual exemplars are similar to the real

exemplars; (2) The generated virtual exemplars are discriminative for classification; (3) For ZSL, the generator trained on seen classes is semantically transferable, so that it could be applied for unseen classes. To meet the three requirements, different generative algorithms [56], [57], classification regularizations [48], [62], and semantic regularizations [96], [97], [98], [99], [100], [101] have been designed in recent years. According to generative algorithm, we classify EAGMs into four categories, *i.e.*, GAN-based methods, VAE-based methods, VAEGAN-based methods, and others, which are shown in Figure 2. A review for representative models of each category is then presented.

### 3.2.1 Review for GAN-Based Methods

GAN [57] consists of a generator that synthesizes fake samples and a discriminator that distinguishes fake samples from real samples. Because the standard GAN suffers from a difficult training process, Arjovsky *et al.* [56] applied the Wasserstein distance and constructed the Wasserstein GAN (WGAN) to improve learning stability. Based on WGAN, Xian *et al.* [48] designed the initial feature-generating model, *i.e.*, f-CLSWGAN, which generated discriminative features by using an external pretrained softmax classifier. Li *et al.* [102] introduced soul samples as the meta-representation of one class into the proposed LisGAN. Through regularizing that each generated sample should be close to at least one soul sample, the model provided a more reliable generative zero-shot learning. Meanwhile, at the recognition stage, Li *et al.* [102] proposed to use two classifiers, which were deployed in a cascade way, to achieve a coarse-to-fine result. Considering that generative models were trained using seen dataset and were expected to implicitly transfer knowledge from seen to unseen classes, Vyas *et al.* [103] proposed the LsrGAN model, which leveraged the semantic relationship between seen and unseen categories by incorporating a novel semantic regularized loss. The regularized LsrGAN was required to generate visual features that mirrored the semantic relationships between seen and unseen classes and hence was more applicable for unseen classes.

### 3.2.2 Review for VAE-Based Methods

VAE [59] is also a popular generative model, which uses an encoder that represents the input as a latent variable with a Gaussian distribution assumption and a decoder that reconstructs the input from the latent variable. Mishra *et al.* [104] first used a conditional variational autoencoder (CVAE) to generate virtual samples from given attributes and applied the generated samples to train a SVM for

unseen classes. In GZSL, to reduce the bias towards seen data, the SVM uses the data generated from both seen and unseen classes as opposed to using the real data for seen classes. Similarly, to address the bias problem, Schonfeld *et al.* [79] proposed the CADA-VAE model, where a shared latent space of visual features and semantic features was learned by modality specific aligned variational autoencoders. The key to CADA-VAE was that the distributions learned from visual features and from semantic information were aligned to construct latent features that contained the essential multi-modal information associated with unseen classes. Meanwhile, because VAEs can only optimize the lower bound on the log-likelihood of observed data, Gu *et al.* [105] proposed a conditional version of generative flow (GF), namely VAE-cFlow model. By using VAE, the semantic features are firstly encoded into tractable latent distributions, conditioned on that the generative flow optimizes the exact log-likelihood of the observed visual features for improved generation ability.

### 3.2.3 Review for VAEGAN-Based Methods

VAEGAN [106], which is a combination of VAE and GAN, is also applied for ZSL and FSL. Xian *et al.* [67] proposed the f-VAEGAN-D2 model to combine the strengths of VAE and GAN for feature generation. In addition, via an unconditional discriminator, f-VAEGAN-D2 learns the marginal feature distribution of unlabeled samples for transductive learning. Narayan *et al.* [107] introduced a feedback loop into VAEGAN and proposed the tf-VAEGAN model. The latent embeddings from the feedback loop together with the corresponding synthesized features were transformed into discriminative features and utilized during classification to reduce ambiguities among categories. Similarly, Chen *et al.* [68] proposed a simple yet effective GZSL method, termed FREE, to tackle the cross-dataset bias problem. FREE employed a feature refinement module to refine the visual features of seen and unseen classes and used a self-adaptive margin center loss to guide the model to learn semantically and class-relevant representations. An interesting application of the VAEGAN for GZSL was the GCM-CF by Yue *et al.* [108], which proposed a novel counterfactual faithful framework. GCM-CF applied the consistence rule to perform unseen/seen binary classification by asking whether a virtual sample of VAEGAN is counterfactual faithful or not. If a sample was classified into seen classes, the conventional supervised learning classifier could be applied; otherwise for ZSL, the conventional ZSL classifier was applied.

### 3.2.4 Review for Other Methods

Apart from GANs, VAEs, and VAEGANs, a few studies have attempted to synthesize visual features with other generative algorithms. For examples, Shen *et al.* [109] incorporated the flow-based models into ZSL and proposed the invertible zero-shot flow to learn factorized data embeddings with the forward pass of an invertible flow network. The mentioned VAE-cFlow [105] can also be treated as a flow-based model. Feng *et al.* [38] constructed a generative model with local and global relation knowledge and addressed the bias problem using a transfer increment strategy. Because these paradigms for ZSL and GZSL have not been studied by suf-

ficient methods, we focus on GAN-, VAE-, and VAEGAN-based EAGMs in this paper.

## 4 EVALUATED METHODS

Here, we describe the specific models evaluated in this work.

### 4.1 GAN-Based Methods

#### 4.1.1 f-CLSWGAN

f-CLSWGAN proposed by Xian *et al.* [48] is the classic feature generation model, whose objective is:

$$\mathcal{L}_{fclswgan} = \mathcal{L}_{wgan} + \beta \mathcal{L}_{cls}, \quad (7)$$

and

$$\mathcal{L}_{wgan} = \mathbb{E}[D(x_s, a_s)] - \mathbb{E}[D(\tilde{x}_s, a_s)] + \lambda \mathbb{E}[(\|\nabla_{\tilde{x}_s} D(\tilde{x}_s, a_s)\|_2 - 1)^2], \quad (8)$$

$$\mathcal{L}_{cls} = -\mathbb{E}[\log p(y_s | \tilde{x}_s)], \quad (9)$$

where  $\tilde{x}_s = G(a_s, z)$ ,  $\hat{x}_s = \alpha x_s + (1 - \alpha)\tilde{x}_s$  with  $\alpha \sim \mathcal{U}(0, 1)$ ,  $\beta$  and  $\lambda$  are penalty coefficients, and  $D$  and  $G$  are discriminator and generator of WGAN, respectively. The  $\mathcal{L}_{wgan}$  implements the adversarial training for feature generation and the  $\mathcal{L}_{cls}$  makes the generated feature discriminative for classification. In f-CLSWGAN, a one-layer softmax network is used as the final classifier.

#### 4.1.2 LisGAN

LisGAN proposed by Li *et al.* [102] introduces several soul samples for each class to guide the feature generation process. The soul sample is defined as the mean of a cluster of samples. The objective of LisGAN is:

$$\mathcal{L}_{lisgan} = \mathcal{L}_{wgan} + \beta \mathcal{L}_{cls} + \delta \mathcal{L}_{r1} + \gamma \mathcal{L}_{r2}, \quad (10)$$

and

$$\mathcal{L}_{r1} = \frac{1}{\tilde{N}_s} \sum_{j=1, i \in \mathcal{Y}_s}^{\tilde{N}_s} \min_{k \in [1, K]} \|\tilde{x}_s^{(j)} - \mu_{s_i}^{(k)}\|_2^2, \quad (11)$$

$$\mathcal{L}_{r2} = \frac{1}{p} \sum_{i=1}^p \min_{k \in [1, K]} \|\tilde{\mu}_{s_i}^{(k)} - \mu_{s_i}^{(k)}\|_2^2, \quad (12)$$

where  $\tilde{N}_s$  is the number of generated samples,  $K$  is the number of soul samples,  $\mu_{s_i}^{(k)}$  is the  $k$ -th soul sample of the  $i$ -th seen classes, and  $\delta$  and  $\gamma$  are penalty coefficients. The  $\mathcal{L}_{r1}$  and  $\mathcal{L}_{r2}$  require the generated sample and the virtual soul sample to be close to at least one soul sample. Besides, in the final classification stage, LisGAN uses two classifiers in a cascade style to achieve a coarse-to-fine result.

#### 4.1.3 LsrGAN

LsrGAN proposed by Vyas *et al.* [103] introduces a SR-Loss to require the generated visual features to mirror the semantic relationships among classes. The objective of LsrGAN is:

$$\mathcal{L}_{lsrgan} = \mathcal{L}_{wgan} + \beta \mathcal{L}_{cls} + \delta \mathcal{L}_{sr1} + \gamma \mathcal{L}_{sr2}, \quad (13)$$

and

$$\mathcal{L}_{sr1} = \frac{1}{p} \sum_{i=1}^p \sum_{j=1}^p \left[ \left\| \max(0, C(\mu_{s_j}, \tilde{\mu}_{s_i}) - (C(a_{s_j}, a_{s_i}) + \epsilon)) \right\|_2^2 + \left\| \max(0, (C(a_{s_j}, a_{s_i}) - \epsilon) - C(\mu_{s_j}, \tilde{\mu}_{s_i})) \right\|_2^2 \right], \quad (14)$$

TABLE 3  
Comparison of Evaluated Models

NO. Model	Paper		Generative Model		Novel Regularization			Classification		Additional Techniques
	Conf. Year	Type	Loss	Discrim.	Generat.	Vis.-Sem.	Classifier	Train. Input Data		
1 f-CLSWGAN [48]	CVPR 2018	WGAN	$\mathcal{L}_{wgan}$	$\mathcal{L}_{cls}$	—	—	Softmax	$x_s \cup \tilde{x}_u$	—	
2 LisGAN [102]	CVPR 2019	WGAN	$\mathcal{L}_{wgan}$	$\mathcal{L}_{cls}$	$\mathcal{L}_{r1} + \mathcal{L}_{r2}$	—	Softmax	$x_s \cup \tilde{x}_u$	Two-step classification	
3 LsrGAN [103]	ECCV 2020	WGAN	$\mathcal{L}_{wgan}$	$\mathcal{L}_{cls}$	—	$\mathcal{L}_{sr1} + \mathcal{L}_{sr2}$	Softmax	$x_s \cup \tilde{x}_u$	—	
4 CVAE [104]	CVPR 2017	CVAE	$\mathcal{L}_{cvae}$	—	—	—	SVM	$\tilde{x}_s \cup \tilde{x}_u$	—	
5 CADA-VAE [79]	CVPR 2019	VAE	$\mathcal{L}_{xvae} + \mathcal{L}_{avae}$	—	$\mathcal{L}_{ca}$	$\mathcal{L}_{da}$	Softmax	$h_{sx} \cup \tilde{h}_{ux}$	Warm-up stage	
6 VAE-cFlow [105]	CVPR 2020	GF/VAE	$\mathcal{L}_{flow} + \mathcal{L}_{vae}^{flow}$	$\mathcal{L}_{hcls}$	—	—	Softmax	$x_s \cup \tilde{x}_u$	Temperature scaling	
7 f-VAEGAN-D2 [67]	CVPR 2019	VAEGAN	$\mathcal{L}_{vaeagan}$	—	$\mathcal{L}_{wgan}^u$	—	Softmax	$x_s \cup \tilde{x}_u$	—	
8 tf-VAEGAN [107]	ECCV 2020	VAEGAN	$\mathcal{L}_{vaeagan}$	—	—	$\mathcal{L}_{cyc}$	Softmax	$x_s \cup h_s \cup \tilde{x}_u \cup \tilde{h}_u$	Feed-back loop	
9 FREE [68]	ICCV 2021	VAEGAN	$\mathcal{L}_{vaeagan}$	$\mathcal{L}_{samc}$	—	$\mathcal{L}_{cyc}$	Softmax	$x_s \cup h_s \cup \hat{a}_s \cup \tilde{x}_u \cup \tilde{h}_u \cup \tilde{a}_u$	—	
10 GCM-CF [108]	CVPR 2021	VAEGAN	$\mathcal{L}_{vaeagan}$	$\mathcal{L}_y$	—	—	Softmax	$x_s \cup h_s \cup \tilde{x}_u \cup \tilde{h}_u$	Counterfactual inference	

$$\mathcal{L}_{sr2} = \frac{1}{q} \sum_{i=1}^q \sum_{j=1}^p [||\max(0, C(\mu_{sj}, \tilde{\mu}_{ui}) - (C(a_{sj}, a_{ui}) + \epsilon))||_2^2 + ||\max(0, (C(a_{sj}, a_{ui}) - \epsilon) - C(\mu_{sj}, \tilde{\mu}_{ui}))||_2^2], \quad (15)$$

where  $\mu$  is the mean of a class's visual features,  $C$  is the cosine similarity, and  $\epsilon$  is the given error bound. The  $\mathcal{L}_{sr1}$  and  $\mathcal{L}_{sr2}$  are performed in the seen scope and between seen and unseen scopes, respectively, which require the visual relationships among classes to be similar to semantic relationships. The one-layer softmax classifier is also used for LsrGAN.

## 4.2 VAE-Based Methods

### 4.2.1 CVAE

CVAE, which consists of an encoder,  $E$ , and a decoder,  $G$ , is first used by Mishra *et al.* [104] to generate unseen visual features. The objective of CVAE in ZSL is:

$$\mathcal{L}_{cvae} = \mathcal{L}_{kl} + \beta \mathcal{L}_{rec}, \quad (16)$$

and

$$\mathcal{L}_{kl} = KL(q(h_s|a_s)||p(h_s|x_s, a_s)), \quad (17)$$

$$\mathcal{L}_{rec} = -\mathbb{E}[\log p(x_s|h_s, a_s)], \quad (18)$$

where  $h_s = E(x_s, a_s)$  is the hidden feature of CVAE. The  $\mathcal{L}_{kl}$  requires  $h_s$  to follow the given distribution and the  $\mathcal{L}_{rec}$  reconstructs the input sample from the hidden feature, *i.e.*,  $\tilde{x}_s = G(h_s, a_s)$ . In CVAE, SVM is used as the final classifier. For GZSL, the data generated from both seen and unseen classes are used for training to reduce the bias towards seen classes.

### 4.2.2 CADA-VAE

CADA-VAE proposed by Schonfeld *et al.* [79] aligns two VAEs, *i.e.*, xVAE and aVAE, to learn a shared latent space of visual features and semantic features. The objective of CADA-VAE is:

$$\mathcal{L}_{cadavae} = \mathcal{L}_{xvae} + \mathcal{L}_{avae} + \delta \mathcal{L}_{ca} + \gamma \mathcal{L}_{da}, \quad (19)$$

and

$$\mathcal{L}_{xvae} = KL(q(h_{sx})||p(h_{sx}|x_s)) - \beta \mathbb{E}[\log p(x_s|h_{sx})], \quad (20)$$

$$\mathcal{L}_{avae} = KL(q(h_{sa})||p(h_{sa}|a_s)) - \beta \mathbb{E}[\log p(a_s|h_{sa})], \quad (21)$$

$$\mathcal{L}_{ca} = |x_s - G_x(E_a(a_s))| + |a_s - G_a(E_x(x_s))|, \quad (22)$$

$$\mathcal{L}_{da} = (||\mu_{h_{sa}} - \mu_{h_{sx}}||_2^2 + ||\sigma_{h_{sa}}^{\frac{1}{2}} - \sigma_{h_{sx}}^{\frac{1}{2}}||_2^2)^{\frac{1}{2}}, \quad (23)$$

where  $h$  is the hidden feature of VAE, and  $\mu$  and  $\sigma$  are the mean and variance of  $h$ . The  $\mathcal{L}_{xvae}$  and  $\mathcal{L}_{avae}$  train two VAEs for  $x$  and  $a$ , respectively, the  $\mathcal{L}_{ca}$  performs a cross-modal reconstruction, and the  $\mathcal{L}_{da}$  aligns two hidden spaces to overcome the bias between visual and semantic features. In CADA-VAE, the one-layer softmax network is used as the final classifier.

### 4.2.3 VAE-cFlow

VAE-cFlow proposed by Gu *et al.* [105] uses the GF model to accurately estimate the log-likelihood of observed data. The objective of VAE-cFlow is:

$$\mathcal{L}_{vaeeflow} = \mathcal{L}_{flow} + \delta \mathcal{L}_{vae}^{flow} + \gamma \mathcal{L}_{hcls}, \quad (24)$$

and

$$\begin{aligned} \mathcal{L}_{flow} &= -\mathbb{E}[\log p(x_s|a_s)] \\ &= -\mathbb{E}[\log p(h_{sf}|a_s) + \log(|\det(\frac{dh_{sf}}{dx_s})|)], \end{aligned} \quad (25)$$

$$\mathcal{L}_{vae}^{flow} = -\mathbb{E}[\log p(a_s|h_{sf})] + \sum (\sigma_{h_{sf}}^2 - \log \sigma_{h_{sf}}^2 - 1), \quad (26)$$

$$\mathcal{L}_{hcls} = -\mathbb{E}[\log p(y_s|h_s)], \quad (27)$$

where  $h_s$  is the hidden feature of VAE for  $a_s$ ,  $h_{sf}$  is the scaled  $h_s$ . The  $\mathcal{L}_{flow}$  trains an invertible generative model between  $h_{sf}$  and  $x_s$ , while the  $\mathcal{L}_{vae}^{flow}$  trains a VAE model without the zero-mean restriction to encode  $a_s$  to  $h_s$ . The  $\mathcal{L}_{hcls}$  is applied on  $h_s$  to encourage the separation of different classes. The one-layer softmax network is used for VAE-cFlow.

## 4.3 VAEGAN-Based Methods

### 4.3.1 f-VAEGAN-D2

f-VAEGAN-D2 proposed by Xian *et al.* [67] combines the strength of CVAE and WGAN. In f-VAEGAN-D2, the decoder of VAE is the generator of WGAN. The objective of f-VAEGAN-D2 is:

$$\begin{aligned} \mathcal{L}_{fvaegand2} &= \mathcal{L}_{vaeagan} + \gamma \mathcal{L}_{wgan}^u \\ &= \mathcal{L}_{wgan} + \delta \mathcal{L}_{cvae} + \gamma \mathcal{L}_{wgan}^u, \end{aligned} \quad (28)$$

and

$$\begin{aligned} \mathcal{L}_{wgan}^u &= \mathbb{E}[D(x_u)] - \mathbb{E}[D(\tilde{x}_u)] \\ &\quad + \lambda \mathbb{E}[(||\nabla_{\tilde{x}_u} D(\tilde{x}_u)||_2 - 1)^2], \end{aligned} \quad (29)$$

where  $\mathcal{L}_{wgan}^u$  is applied for the transductive learning of unseen classes. In this paper, we only consider the inductive learning setting, and f-VAEGAN-D2 is performed without  $\mathcal{L}_{wgan}^u$ . The one-layer softmax network is used for classification.

#### 4.3.2 tf-VAEGAN

tf-VAEGAN proposed by Narayan *et al.* [107] introduces a feedback loop into VAEGAN. The objective of tf-VAEGAN is:

$$\mathcal{L}_{tfvaeagan} = \mathcal{L}_{vaeagan} + \gamma \mathcal{L}_{cyc}, \quad (30)$$

and

$$\mathcal{L}_{cyc} = \mathbb{E}[|Dec(x_s) - a_s| + |Dec(\tilde{x}_s) - a_s|], \quad (31)$$

where  $Dec$  is a decoder to obtain  $\hat{a}_s = Dec(x_s)$  and  $\tilde{a}_s = Dec(\tilde{x}_s)$ . The  $\mathcal{L}_{cyc}$  reconstructs the sample back to its semantic description. The latent feature  $h_s$  in reconstruction is used as a part of generator input, which enhances the virtual features' semantical consistence. In tf-VAEGAN, the one-layer softmax network is used as the final classifier.

#### 4.3.3 FREE

FREE proposed by Chen *et al.* [68] uses a new SAMC loss to learn class- and semantically relevant representations. The objective of FREE is:

$$\mathcal{L}_{free} = \mathcal{L}_{vaeagan} + \gamma \mathcal{L}_{cyc} + \xi \mathcal{L}_{samc}, \quad (32)$$

and

$$\mathcal{L}_{samc} = \max(0, \Delta + \eta \|\mu_s - c_y\|_2^2 - (1 - \eta) \|\mu_s - c_{y'}\|_2^2), \quad (33)$$

where  $\mu_s$  is encoded from the hidden feature  $h_s$  in the reconstruction by  $\mathcal{L}_{cyc}$ ,  $\Delta$ ,  $\xi$ , and  $\eta$  are given coefficients,  $c_y$  is the trainable center of class  $y$ , and  $c_{y'}$  is the center of another class. The  $\mathcal{L}_{samc}$  makes  $\mu_s$  intra-class contraction and inter-class separation. FREE also uses the softmax classifier for final classification.

#### 4.3.4 GCM-CF

GCM-CF proposed by Yue *et al.* [108] designs a novel counterfactual inference framework. The objective of GCM-CF is:

$$\mathcal{L}_{gcmcf} = \mathcal{L}_{vaeagan} + \gamma \mathcal{L}_y, \quad (34)$$

and

$$\mathcal{L}_y = -\log \frac{\exp(-dist(x_s, \tilde{x}_s))}{\sum_{\tilde{x}'_s \in \tilde{\mathcal{X}}'_s \cup \{\tilde{x}_s\}} \exp(-dist(x_s, \tilde{x}'_s))}, \quad (35)$$

where  $dist$  denotes Euclidean distance and  $\tilde{x}'_s$  is the generated counterfactual samples. Based on the designed counterfactual inference rules, GCM-CF performs unseen/seen binary classification for a test sample. And the tf-VAEGAN model would be applied for the final supervised or ZSL classification.

For clarification, the reviewed ten models are listed and compared in Table 3, where the mentioned regularizations are categorized into the discriminative items (Discrim.), generative items (Generat.), and visual-semantic items (Vis.-Sem.).

## 5 EMBEDDING MODIFICATIONS

Here, we modify the benchmarked embeddings contributed by Xian *et al.* [28] to explore the effects of embeddings on EAGMs in depth, including the visual embedding and semantic embedding.

### 5.1 Modifications on Visual Embedding

#### 5.1.1 Original Features

Currently, the visual features used in benchmark datasets are 2,048-dim top-layer pooling units of ResNet101 [13], which is pretrained on ImageNet 1K and not finetuned. The ResNet features are validated to be more effective than GoogLeNet features [102] and widely used in researches. We name the ResNet features contributed by Xian *et al.* [28] as "original features".

#### 5.1.2 Naive Features

To provide a fair comparison, we reproduce the 2,048-dimensional features with a pretrained ResNet101 network. Specifically, we resize the images in dataset to  $256 \times 256$  and then apply a center cropping function to obtain  $224 \times 224$  images as the input of ResNet101. The 2,048-dim top-layer pooling units are used as the visual representation. We name the reproduced visual features as "naive features".

#### 5.1.3 Finetuned Features

We finetune the pretrained ResNet101 on the seen classes of each dataset. Note that only the images in training set are used and the splits proposed by Xian *et al.* [28] are followed to make the zero-shot setting effective. The training loss is:

$$\mathcal{L}_{ce} = -\mathbb{E}[\log p(y_s|x_s)]. \quad (36)$$

We observe that the SGD optimizer is more effective than the Adam optimizer [113]. The momentum of SGD is set to 0.9. The learning rate is initialized to 0.01, and a linear learning rate decay scheduler is used to decrease the learning rate by 0.1 every 7 rounds for better convergence. We name the features as "finetuned features". In comparison with the naive features, the finetuned features contain more visual information of the benchmark dataset.

#### 5.1.4 Regularized Features

We also finetune the pretrained ResNet101 with a semantic regularization item. The training loss is:

$$\mathcal{L}_{re} = \mathcal{L}_{ce} + \alpha \mathcal{L}_{se}, \quad (37)$$

and

$$\mathcal{L}_{se} = \max(0, \Delta + \lambda C(x_s, a_s) - (1 - \lambda)C(x_s, a'_s)), \quad (38)$$

where  $\Delta$ ,  $\alpha$ , and  $\lambda$  are given coefficients,  $a_s$  is the semantic description of  $x_s$ ,  $a'_s$  is the semantic description of another class, and  $C$  is the cosine similarity. In comparison with conventional triplet loss, the  $\mathcal{L}_{se}$  makes the visual feature  $x_s$  align with its semantic description  $a_s$  and misalign with other descriptions. We name the features as "regularized features". In comparison with the finetuned features, regularized features contain semantic information of the benchmark dataset.



## 5.2 Modifications on Semantic Embedding

### 5.2.1 Original Descriptions

The character-based CNN-RNN model [25] is currently used to obtain the benchmarked 1,024-dimensional semantic embedding. We name the semantic descriptions contributed by Xian *et al.* [28] as “original descriptions”. Meanwhile, we note that some datasets [15], [28], [110], [111] use manually annotated attributes as semantic embedding. Since the modifications of manually annotated attributes depend on experience and have little algorithm contribution, we pay few attentions on them in this work.

### 5.2.2 Naive Descriptions

Similarly, to provide a fair comparison, we reproduce the character-based CNN-RNN model to obtain the 1,024-dimensional descriptions. The backbone of the model’s image feature extractor is GoogLeNet [102], and the backbone of the model’s text feature extractor is LSTM [114]. We use the texts and class splits contributed by Xian *et al.* [28]. The symmetrical training loss of the character-based CNN-RNN model is:

$$\mathcal{L}_{dssje} = \mathcal{L}_{xsje} + \mathcal{L}_{asje}, \quad (39)$$

and

$$\mathcal{L}_{xsje} = \max_{y \in \mathcal{Y}_s} (0, \Gamma(y_s, y) + \mathbb{E}_{a \in \mathcal{A}_s} [C(x_s, a) - C(x_s, a_s)]), \quad (40)$$

$$\mathcal{L}_{asje} = \max_{y \in \mathcal{Y}_s} (0, \Gamma(y_s, y) + \mathbb{E}_{x \in \mathcal{X}_s} [C(x, a_s) - C(x_s, a_s)]), \quad (41)$$

where  $\Gamma$  is the 0-1 loss and  $C$  is the cosine similarity. The  $\mathcal{L}_{xsje}$  and  $\mathcal{L}_{asje}$  optimize the visual-semantic compactness based on  $x_s$  and  $a_s$ , respectively. The average hidden features of LSTM are used as the semantic descriptions for each class and are named as “naive descriptions”.

### 5.2.3 GRU-based Descriptions

To follow the zero-shot principle, the character-based CNN-RNN model is trained on seen classes and applied to obtain all classes’ semantic descriptions. As discussed in previous researches on conventional ZSL, this paradigm suffers from a bias problem towards seen classes during predicting for unseen classes. In experiments, we notice that using GRU [115] replaces LSTM as the backbone of text feature extractor could alleviate the model’s overfitting on seen classes with fewer parameters and contributes to performance improvement. We name the 1,024-dimensional features from the modified character-based CNN-GRU model as “GRU-based descriptions”.

### 5.2.4 Imbalanced GRU-based Descriptions

The character-based CNN-GRU model enjoys a balanced training loss, *i.e.*,  $\mathcal{L}_{dssje}$ , which equally treats the visual features,  $x_s$ , and the semantic features,  $a_s$ , by  $\mathcal{L}_{xsje}$  and  $\mathcal{L}_{asje}$ , respectively. However, we note that the aim of the character-based CNN-GRU for ZSL is the semantic features, and the visual features of the model are usually not used for other models. The semantic feature-based loss deserves more attentions in model training. Hence, the objective of the character-based CNN-GRU is modified as:

$$\mathcal{L}_{disje} = (1 - \alpha)\mathcal{L}_{xsje} + \alpha\mathcal{L}_{asje}, \quad (42)$$

where  $\alpha > 0.5$  is the given weight. We name the 1,024-dimensional features from the character-based CNN-GRU model trained by  $\mathcal{L}_{disje}$  as “imbalanced GRU-based descriptions”.

TABLE 4  
Statistics of the Five Benchmark Datasets

Dataset	#A	Class number		Image number		
		# $\mathcal{Y}_s$	# $\mathcal{Y}_u$	Total	# $\mathcal{X}_s$	# $\mathcal{X}_u$
FLO	1024	82	20	8189	7034	1155
CUB	312	150	50	11788	8821	2967
SUN	102	645	72	14340	12900	1440
AWA2	85	40	10	37322	29409	7913
AWA	85	40	10	30475	25517	4958

TABLE 5  
Comparison of Visual and Semantic Embeddings

Scope	Embedding	Information Source	Dataset
$\mathcal{X}$	Original	ImageNet	FLO,CUB,SUN,AWA2,AWA
	Naive	ImageNet	FLO,CUB,SUN,AWA2
	Finetuned	ImageNet + Seen images	FLO,CUB,SUN,AWA2
	Reg.	ImageNet + Seen images + Descrip.	FLO,CUB,SUN,AWA2
Scope	Embedding	Model	Dataset
$\mathcal{A}$	Original	CNN-RNN/Att.	FLO/CUB,SUN,AWA2,AWA
	Naive	CNN-RNN	FLO
	GRU.	CNN-GRU	FLO
	Imb. GRU.	Imb. CNN-GRU	FLO

Note A: Visual images of AWA are unavailable for research.

Note B: Original embeddings are made by Xian *et al.*, and others are by ourselves.

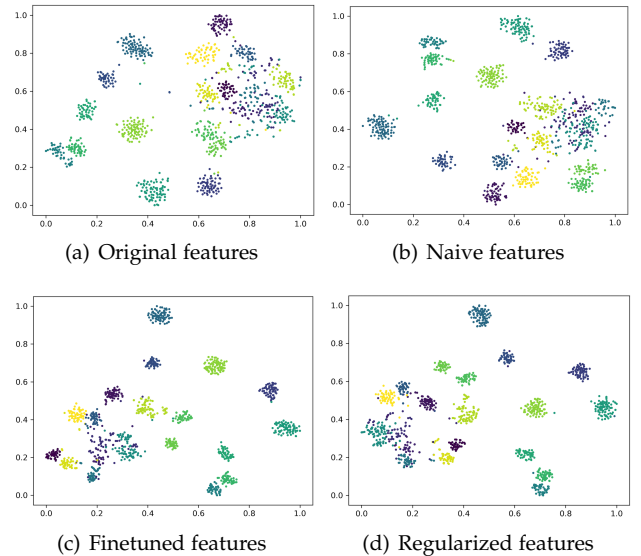


Fig. 3. The visualization of four types of visual features on the unseen classes of FLO.

## 6 EXPERIMENTS

### 6.1 Experiment Settings

#### 6.1.1 Benchmark Dataset

In this paper, five benchmark datasets are used for experiments, including the Oxford Flowers (FLO) dataset [26], the Caltech-UCSD-Birds (CUB) dataset [110], the SUN attributes (SUN) dataset [111], the Animals with Attributes2 (AWA2) dataset [28], and the Animals with Attributes (AWA) dataset

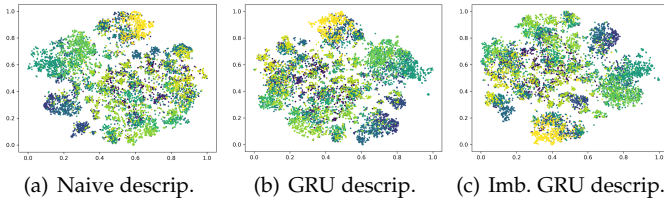


Fig. 4. The sample-level visualization of three types of semantic descriptions on the unseen classes of FLO.

TABLE 6  
Splits for ZSL and FSL

Task	Scope	FLO	CUB	SUN	AWA2	AWA	
ZSL	Tr	$\#\mathcal{X}_s$	7034	8821	12900	29409	25517
		$\#\mathcal{X}_u$	-	-	-	-	-
	Te	$\#\mathcal{X}_s$	-	-	-	-	-
		$\#\mathcal{X}_u$	1155	2967	1440	7913	5685
GZSL	Tr	$\#\mathcal{X}_s$	5631	7057	10320	23527	19832
		$\#\mathcal{X}_u$	-	-	-	-	-
	Te	$\#\mathcal{X}_s$	1403	1764	2580	5882	4958
		$\#\mathcal{X}_u$	1155	2967	1440	7913	5685
UFSL	Tr	$\#\mathcal{X}_s$	7034	8821	12900	29409	25517
		$\#\mathcal{X}_u$	$N_q$	$N_q$	$N_q$	$N_q$	$N_q$
	Te	$\#\mathcal{X}_s$	-	-	-	-	-
		$\#\mathcal{X}_u$	$1155-N_q$	$2967-N_q$	$1440-N_q$	$7913-N_q$	$5685-N_q$
GUFSL	Tr	$\#\mathcal{X}_s$	5631	7057	10320	23527	19832
		$\#\mathcal{X}_u$	$N_q$	$N_q$	$N_q$	$N_q$	$N_q$
	Te	$\#\mathcal{X}_s$	1403	1764	2580	5882	4958
		$\#\mathcal{X}_u$	$1155-N_q$	$2967-N_q$	$1440-N_q$	$7913-N_q$	$5685-N_q$
SFSL	Tr	$\#\mathcal{X}_s$	$N_p$	$N_p$	$N_p$	$N_p$	$N_p$
		$\#\mathcal{X}_u$	-	-	-	-	-
	Te	$\#\mathcal{X}_s$	-	-	-	-	-
		$\#\mathcal{X}_u$	1155	2967	1440	7913	5685
GSFSL	Tr	$\#\mathcal{X}_s$	$N_p$	$N_p$	$N_p$	$N_p$	$N_p$
		$\#\mathcal{X}_u$	-	-	-	-	-
	Te	$\#\mathcal{X}_s$	1403	1764	2580	5882	4958
		$\#\mathcal{X}_u$	1155	2967	1440	7913	5685

[15]. FLO contains 8,189 flower images from 102 different categories. CUB is a fine-grained dataset, which contains 11,788 images from 200 kinds of birds. SUN is a subset of the SUN scene dataset with fine-grained attributes, which contains 14,340 images from 717 types of scenes. AWA2 and AWA are classic image datasets and include fifty types of animals. AWA2 has 37,322 images and AWA has 30,475 images. Note that the original images of AWA are unavailable for research, but the features of AWA are contributed by Xian *et al.* [27]. The statistics of the five datasets are summarized in Table 4.

### 6.1.2 Embedding features

The visual features and semantic descriptions used for experiments have been discussed in last section, and they are listed and compared in Table 5 for clarification. Besides, we visualize the visual features and semantic features on the unseen classes of FLO by t-SNE algorithm [116] for intuitive comparison. The visualization of four types of visual features is shown in Figure 3, and the sample-level visualization of three types of semantic features is shown in Figure 4. Note that Xian *et al.* [28] did not contribute the sample-level semantic features of original descriptions. Hence, the original descriptions are not visualized here. From Figure 3 and Figure 4, we can observe that the distributions of these features are very different, though they are obtained in a similar paradigm.

### 6.1.3 Dataset Splits

For ZSL and GZSL, we use the proposed splits by Xian *et al.* [27], which strictly follow the disjoint-class principle for seen and unseen classes. Based on the splits of ZSL and GZSL, we select  $N$  samples from each unseen class and add them into the training set for UFSL and GUFSL. Meanwhile, the selected unseen samples are removed from the test set. For SFSL and GSFSL, we only retain  $N$  samples for each seen class in the training set. The other samples in the training set are abandoned and not added into the test set for an intuitive comparison with ZSL and GZSL. The specific splits for ZSL, GZSL, UFSL, GUFSL, SFSL, and GSFSL are listed in Table 6.

TABLE 7  
Comparison of Reproduced Results and Results From the Original Publications on ZSL and GZSL

Model	Type	FLO		CUB		SUN		AWA2		AWA	
		Z	H	Z	H	Z	H	Z	H	Z	H
f-CLS.	O	67.2	65.6	57.3	49.7	60.8	39.4	-	-	68.2	59.6
	R	67.6	68.5	56.3	49.8	60.1	39.2	-	-	67.4	59.3
	B	+0.4	+2.9	-1.0	+0.1	-0.7	-0.2	-	-	-0.8	-0.3
Lis.	O	69.6	68.3	58.8	51.6	61.7	40.2	-	-	70.6	62.3
	R	68.3	67.4	57.3	51.1	61.2	40.0	-	-	67.9	61.0
	B	-1.3	-0.9	-1.5	-0.5	-0.5	-0.2	-	-	-2.7	-1.3
Lsr.	O	-	-	60.3	53.0	62.5	40.9	-	-	66.4	63.0
	R	-	-	59.6	52.6	61.0	40.6	-	-	66.0	62.8
	B	-	-	-0.7	-0.4	-1.5	-0.3	-	-	-0.4	-0.2
CVAE	O	-	-	52.1	34.5	61.7	26.7	65.8	51.2	71.4	47.2
	R	-	-	53.1	32.6	58.5	24.6	69.5	50.2	72.6	49.6
	B	-	-	+1.0	-1.9	-3.2	-2.1	+3.7	-1.0	+1.2	+2.4
CADA.	O	-	-	52.4	-	40.6	-	63.9	-	64.1	-
	R	-	-	52.7	-	40.9	-	64.2	-	64.5	-
	B	-	-	+0.3	-	+0.3	-	+0.3	-	+0.4	-
VAE-c.	O	-	-	57.2	52.8	61.8	42.8	66.6	64.5	66.4	62.1
	R	-	-	55.4	51.6	61.9	42.5	65.0	62.5	65.8	61.0
	B	-	-	-1.8	-1.2	+0.1	-0.3	-1.6	-2.0	-0.6	-1.1
f-VAE.	O	67.7	64.6	61.0	53.6	64.7	41.3	-	-	71.1	63.5
	R	65.5	68.0	60.3	53.2	63.3	39.9	-	-	73.1	62.5
	B	-2.2	+3.4	-0.7	-0.4	-1.4	-1.4	-	-	+2.0	-1.0
tf-VAE.	O	70.8	71.7	64.9	58.1	66.0	43.0	-	-	72.2	66.6
	R	70.4	71.8	64.4	57.5	65.8	42.2	-	-	71.7	65.8
	B	-0.4	+0.1	-0.5	-0.6	-0.2	-0.8	-	-	-0.5	-0.8
FREE	O	-	75.0	-	57.7	-	41.7	-	67.1	-	66.0
	R	-	74.7	-	56.5	-	41.4	-	67.0	-	65.5
	B	-	-0.3	-	-1.2	-	-0.3	-	-0.1	-	-0.5
GCM.	O	-	-	60.3	-	42.2	-	-	-	-	-
	R	-	-	56.2	-	41.3	-	-	-	-	-
	B	-	-	-4.1	-	-0.9	-	-	-	-	-

Note: "O", "R", and "B" denote the original result, reproduced result, and bias.

### 6.1.4 Evaluation Criteria

For ZSL, UFSL, and SFSL, we evaluate the model performance with two kinds of criteria, including the average perclass top-1 accuracy,  $Z$ , and the training time,  $ZT$ . The accuracy is defined as:

$$Z = \frac{1}{|\mathcal{Y}|} \sum_{i=1}^{|\mathcal{Y}|} \frac{\#\text{correct predictions in } i}{\#\text{samples in } i}, \quad (43)$$

and  $ZT$  is defined as the time (hours) cost by a model to obtain its  $Z$ . For GZSL, GUFSL, and GSFSL, we evaluate the model performance with four kinds of criteria, including the average perclass top-1 accuracy on unseen classes,  $U$ , the average perclass top-1 accuracy on seen classes,  $S$ , the harmonic mean accuracy,  $H$ , and the training time,  $HT$ . The harmonic mean accuracy is defined as

$H = (2 * S * U)/(S + U)$ , and  $HT$  is defined as the time (hours) cost by a model to obtain its best  $H$ . In comparison with other works, we additionally use training time to evaluate the model performance, since the training efficiency is as important as accuracy in practice.

### 6.1.5 Models and Parameters

In this paper, we reproduce and evaluate ten EAGMs, including f-CLSWGAN, LisGAN, LsrGAN, CVAE, CADA-VAE, VAE-cFlow, f-VAEGAN-D2, tf-VAEGAN, FREE, and GCM-CF. For a fair comparison, we finetune the hyperparameters of these models for ZSL and GZSL on the five benchmark datasets. The reproduced results and the results from the original publications are compared in Table 7. As shown, a total of sixty-five results are reproduced, and the average bias is only -0.49%. We highlight the difficulty of reproducing these networks, which are optimized by back-propagation algorithm with numerous hyperparameters and randomness. Meanwhile, it can be observed that a total of fifteen reproduced results are better than the original results, and the average improvement is +1.24%, which shows that these models are reproduced well. In experiments, the hyperparameters of ZSL are applied for UFSL and SFSL without other modifications, and the hyperparameters of GZSL are applied for GUFSL and GSFSL without other modifications. Although the shared hyperparameters do not help to get the best results for UFSL, SFSL, GUFSL, and GSFSL, they indeed contribute to present a fair comparison among different models and tasks.

## 6.2 Embedding Evaluation on Zero-Shot Learning

Here, we show the effects of visual and semantic embeddings on EAGMs for ZSL and GZSL.

### 6.2.1 Visual Embedding

In last section, four types of visual embeddings are presented, including the original features, naive features, finetuned features, and regularized features. Note that the  $\alpha$ ,  $\Delta$ , and  $\lambda$  in Eq. (37) and Eq. (38) for regularized features are different for each datasets. The  $\alpha$  is set to 0.01 for FLO, 0.1 for CUB, 0.01 for SUN, and 0.1 for AWA2. The  $\Delta$  is set to 1 for FLO, 0.01 for CUB, 1 for SUN, and 0.1 for AWA2. The  $\lambda$  is set to 0.9 for FLO, 0.99 for CUB, 0.9 for SUN, and 0.9 for AWA2. Based on benchmark datasets, we perform the ZSL and GZSL tasks for EAGMs with the four types of visual embeddings. The results are summarized in Table 8. We analyze the results from five aspects, including the effects of visual embeddings on a single model, the effects on different datasets, the effects on different models, the overall effects, and the model rank.

First, we take the results of f-CLSWGAN on FLO as an example to start our analysis. As shown in Table 8. The change of feature embedding significantly improves both ZSL and GZSL. In comparison with the original features, for ZSL, the naive features, finetuned features, and regularized features show a  $Z$  improvement of 1.8%, 3.8%, and 6.5%. For GZSL, the  $H$  improvement is 1.6%, 9.1%, and 10.2%. Especially, the improvement presented by naive features demonstrates our effective reproduction for the original features. And the improvement presented by finetuned

features and regularized features demonstrates the contributions of adding visual and semantic information for ZSL and GZSL during feature extraction.

Second, we take the results of FLO, CUB, SUN, and AWA2 by f-CLSWGAN as an example to show the effects on different datasets. For ZSL, the best visual features of FLO, CUB, SUN, and AWA2 are the regularized features, regularized features, regularized features, and naive features, respectively. In comparison with the original features, the best features present a  $Z$  improvement of 6.5%, 16.5%, 1.9%, and 2.4%. Meanwhile, we note that the best features of AWA2 is the naive features which demonstrates that adding visual and semantic information of seen classes during feature extraction is not always effective for the accuracy improvement of unseen classes in ZSL. For GZSL, the best visual features are regularized features, and the  $H$  improvement is 10.2%, 18.4%, 3.2%, and 8.7%. We notice that the contribution of regularized features to GZSL is larger than that to ZSL, since GZSL includes seen classes at the test stage. For the training time, the  $ZT$  and  $HT$  are similar.

Third, we take the results of ten EAGMs on FLO as an example to show the effects on different models. For ZSL, the best visual features are the regularized features (f-CLS.), regularized features (Lis.), regularized features (Lsr.), finetuned features (CVAE), regularized features (CADA.), regularized features (VAE-c.), regularized features (f-VAE.), naive features (tf-VAE.), naive features (FREE), naive features (GCM). The best features present a  $Z$  improvement of 6.5%, 9.6%, 5.5%, 14.5%, 6.4%, 11.6%, 4.4%, 4.3%, 0.3%, and 7.7%. For GZSL, the best visual features of tf-VAE. are the finetuned features, and other models' best features are the regularized features. The best features present an  $H$  improvement of 10.2%, 14.2%, 2.7%, 1.4%, 9.9%, 15.1%, 9.8%, 6.5%, 3.9%, and 14.4%. The improvements for ZSL and GZSL demonstrate the positive effects of the given visual features on EAGMs.

Fourth, we list the statistics of Table 8 in Table 9 for intuitive comparison. Based on the results of the ten models, we give the best visual features for each dataset, *i.e.*, regularized features for FLO, CUB, and SUN, and naive features for AWA2. For ZSL, the best features present an average  $Z$  improvement of 6.2%, 13.5%, 0.0%, and 2.3% for FLO, CUB, SUN, and AWA2. For GZSL, the best features present an average  $H$  improvement of 8.8%, 13.6%, 0.5%, and 0.7%. Meanwhile, the highest accuracy for each dataset is also significantly improved by the best features. For ZSL, the best features present a highest  $Z$  improvement of 4.3%, 10.2%, 0.0%, and 5.2% for FLO, CUB, SUN, and AWA2. For GZSL, the highest  $H$  improvements are 6.9%, 11.6%, 0.1%, and 0.3%. These statistics show that the modifications on visual embedding indeed contribute to the EAGM-based ZSL and GZSL.

Finally, we present the ranks of different models with the best and original features, respectively, in Figure 5. When the original visual features are used, f-VAEGAN-D2 and tf-VAEGAN usually present superior performance than other models, whose average ranks are 2.1 and 2.2, respectively. When the best features are used, tf-VAEGAN and LisGAN have superior performance than other models, whose average ranks are 3.0 and 3.4, respectively. In addition, we can observe that f-CLSWGAN and LisGAN show higher



#Rank	Rank										AVE
	1	2	3	4	5	6	7	8	9	10	
f-CLS.			2				2	3	3		7.3
Lis.			1	1	5	2	1				6.1
Lsr.			2	2	3	1	1	1			5.8
CVAE	2								8		8.2
CADA.			2	1	3		2				5.9
VAE-c.	1		1	1			2	2	3	2	6.7
f-VAE.		1		4	1	1		1	2		5.5
tf-VAE.	4	4	1				1				2.1
FREE	3	4	2			1					2.2
GCM.	1	3	1	1			1	2	1		5.2

(a) Original features.

#Rank	Rank										AVE
	1	2	3	4	5	6	7	8	9	10	
f-CLS.	2	1	1	2	1	1					4.3
Lis.	3	1		1	2		1				3.4
Lsr.			1			1	2	1	2	1	7.4
CVAE									3	5	9.6
CADA.			1	1		3	1	2			6.0
VAE-c.	2	1	1		1	1	1	1			5.1
f-VAE.	2	1		2		2	1				4.3
tf-VAE.	3	1	1		2	2	1				3.0
FREE			2	2	2		1			1	5.1
GCM.	1	1				1	2	2	1		6.9

(b) Best features

Fig. 5. Ranks of ten EAGMs. For each model, the ranks of the ten results (five dataset  $\times$  two tasks) from the original features are shown and the ranks of the eight results (four dataset  $\times$  two tasks) from the best features are shown.

TABLE 10  
Effects of Semantic Embeddings on ZSL and GZSL

Type	Method	Emb.	FLO					
			Z	ZT	U	S	H	HT
GAN-based methods	f-CLSWGAN (2018)	Orig.	74.1		69.4	91.0	78.7	
		Naiv.	74.2	0.13	71.1	91.4	79.9	
		GRU.	75.9		<b>74.1</b>	89.7	81.2	0.21
		Imb. GRU.	<b>76.6</b>		72.9	<b>92.0</b>	<b>81.4</b>	
	LisGAN (2019)	Orig.	76.2		71.6	94.8	81.6	
		Naiv.	79.3	0.25	71.9	93.8	81.4	
		GRU.	77.6		72.9	<b>95.6</b>	82.8	0.34
		Imb. GRU.	<b>79.5</b>		<b>73.7</b>	95.4	<b>83.1</b>	
	LsrGAN (2020)	Orig.	74.0		58.5	<b>96.8</b>	72.9	
Naiv.		70.9	0.48	61.7	94.8	74.7		
GRU.		72.4		63.6	95.4	76.2	0.30	
	Imb. GRU.	<b>74.1</b>		<b>65.3</b>	96.1	<b>77.7</b>		
VAE-based methods	CVAE (2017)	Orig.	66.9		16.8	96.2	28.5	
		Naiv.	67.0	0.05	17.6	98.2	29.9	
		GRU.	<b>70.2</b>		17.7	98.1	30.0	0.89
		Imb. GRU.	70.0		<b>17.7</b>	<b>98.3</b>	<b>30.0</b>	
	CADA-VAE (2019)	Orig.	<b>70.4</b>		<b>61.9</b>	90.6	<b>73.5</b>	
		Naiv.	67.8	0.03	51.0	<b>94.2</b>	66.2	
		GRU.	67.6		52.9	94.0	67.7	0.03
		Imb. GRU.	70.0		53.9	93.9	68.5	
	VAE-cFlow (2020)	Orig.	69.0		64.4	90.5	75.3	
Naiv.		69.5	0.16	67.1	87.3	75.9		
GRU.		70.5		68.4	88.9	77.3	0.17	
	Imb. GRU.	<b>72.7</b>		<b>69.1</b>	<b>91.2</b>	<b>78.6</b>		
VAEGAN-based methods	f-VAEGAN-D2 (2019)	Orig.	69.9		66.9	92.9	77.8	
		Naiv.	74.8	0.24	71.6	90.9	80.1	
		GRU.	75.2		<b>73.6</b>	91.1	81.4	0.46
		Imb. GRU.	<b>75.9</b>		72.8	<b>93.0</b>	<b>81.7</b>	
	tf-VAEGAN (2020)	Orig.	70.6		66.5	<b>92.8</b>	77.5	
		Naiv.	73.7	0.23	71.7	87.6	78.9	
		GRU.	74.0		71.8	90.6	80.1	0.18
		Imb. GRU.	<b>74.5</b>		<b>72.3</b>	92.0	<b>81.0</b>	
	FREE (2021)	Orig.	70.8		67.6	<b>93.9</b>	78.6	
Naiv.		72.0	1.83	69.5	91.2	78.9		
GRU.		74.1		70.7	92.3	80.1	1.97	
	Imb. GRU.	<b>75.6</b>		<b>72.4</b>	93.4	<b>81.6</b>		
GCM-CF (2021)	Orig.	61.7		59.9	90.4	72.1		
	Naiv.	67.5	0.75	65.1	<b>91.0</b>	75.9		
	GRU.	<b>69.0</b>		65.2	90.5	75.8	0.72	
	Imb. GRU.	68.3		<b>65.8</b>	89.8	<b>76.0</b>		

change of semantic embedding significantly improves both ZSL and GZSL. For ZSL, the naive descriptions, GRU-based descriptions, and imbalanced GRU-based descriptions show a  $Z$  improvement of 0.1%, 1.8%, and 2.5% in comparison with the original descriptions. For GZSL, the  $H$  improvements are 1.2%, 2.5%, and 2.7%. Meanwhile, six EAGMs obtain their best performance for ZSL and nine EAGMs obtain their best performance for GZSL with the designed imbalanced GRU-based features. In comparison with the original descriptions, the imbalanced GRU-based descriptions averagely improve  $Z$  for ZSL by 3.3% and improve

TABLE 11  
Embeddings Used for the Five Benchmark Datasets in FSL

Task	Emb.	FLO	CUB	SUN	AWA2	AWA
UFSL/GUFSL	$\mathcal{X}$	Reg.	Reg.	Reg.	Naiv.	Orig.
	$\mathcal{A}$	Orig.	Orig.	Orig.	Orig.	Orig.
SFSL/GSFSL	$\mathcal{X}$	Naiv.	Naiv.	Orig.	Naiv.	Orig.
	$\mathcal{A}$	Orig.	Orig.	Orig.	Orig.	Orig.

$H$  for GZSL by 2.3% on the ten EAGMs. These results demonstrate that our modifications on semantic descriptions indeed contribute to EAGM-based ZSL and GZSL.

### 6.3 Baseline of Few-Shot Learning

Here, we show a strong baseline for EAGM-based FSL, including UFSL, GUFSL, SFSL, and GSFSL. The paradigm shown in Eqs. (4)-(6) is used to apply EAGMs for FSL. Five benchmark datasets are used, including FLO, CUB, SUN, AWA2, and AWA. The embeddings used for FSL are listed in Table 11. As shown, for UFSL and GUFSL, we use the best visual embeddings defined in Table 9 for each dataset, which are helpful to obtain satisfactory performance. For SFSL and GSFSL, we use the original or naive visual embeddings to follow the few seen sample principle in the training stage. In addition, we uniformly use the original semantic embeddings for the four few-shot tasks. The few-shot scenarios where one sample, five samples, ten samples, and twenty samples are used for each class are considered. The results of UFSL, GUFSL, SFSL, and GSFSL are summarized in Table 12. We analyze the results from five aspects, including the performance of a single model, the performance on different datasets, the visualization comparison, the model rank, and the effects of imbalanced GRU-based descriptions.

First, we take the results of f-CLSWGAN on FLO as an example to start our analysis. In comparison with the zero-shot scenarios, UFSL and GUFSL improves model performance with a few unseen samples. Specifically, for UFSL, the one-shot, five-shot, ten-shot, and twenty-shot scenarios present a  $Z$  improvement of 0.9%, 1.2%, 15.6%, and 21.4%. For GUFSL, the  $H$  improvement is 0.6%, 9.9%, 15.4%, and 17.4%. Usually, the accuracy is improved with the increasing of the number of unseen samples. The accuracy improvement by more training samples can also be observed on SFSL and GSFSL. In comparison with the one-sample perseen class scenario, the five-shot, ten-shot, and twenty-shot scenarios present a  $Z$  improvement of 12.1%, 19.7%, and 18.0% for SFSL. The  $H$  improvement for GSFSL is 36.1%, 48.2%, and 51.5%. However, the performance of SFSL and GSFSL is inferior to the performance of UFSL, GUFSL, ZSL, and GZSL, since SFSL and GSFSL have only a few seen samples for model training, which are more challenging.

Second, we observe the performance of f-CLSWGAN on FLO, CUB, SUN, AWA2, and AWA. Similarly, the accuracies of UFSL, GUFSL, SFSL, and GSFSL on the five benchmark datasets are usually improved with the increasing of the number of samples. From the one-shot learning to the twenty-shot or ten-shot (SUN) learning, the  $Z$  improvement of UFSL on FLO, CUB, SUN, AWA2, and AWA is 20.5%, 9.6%, 4.0%, 2.4%, and 0.1%, and the  $H$  improvement for GUFSL is 16.8%, 10.9%, 3.5%, 1.1%, and 2.3%. However, the



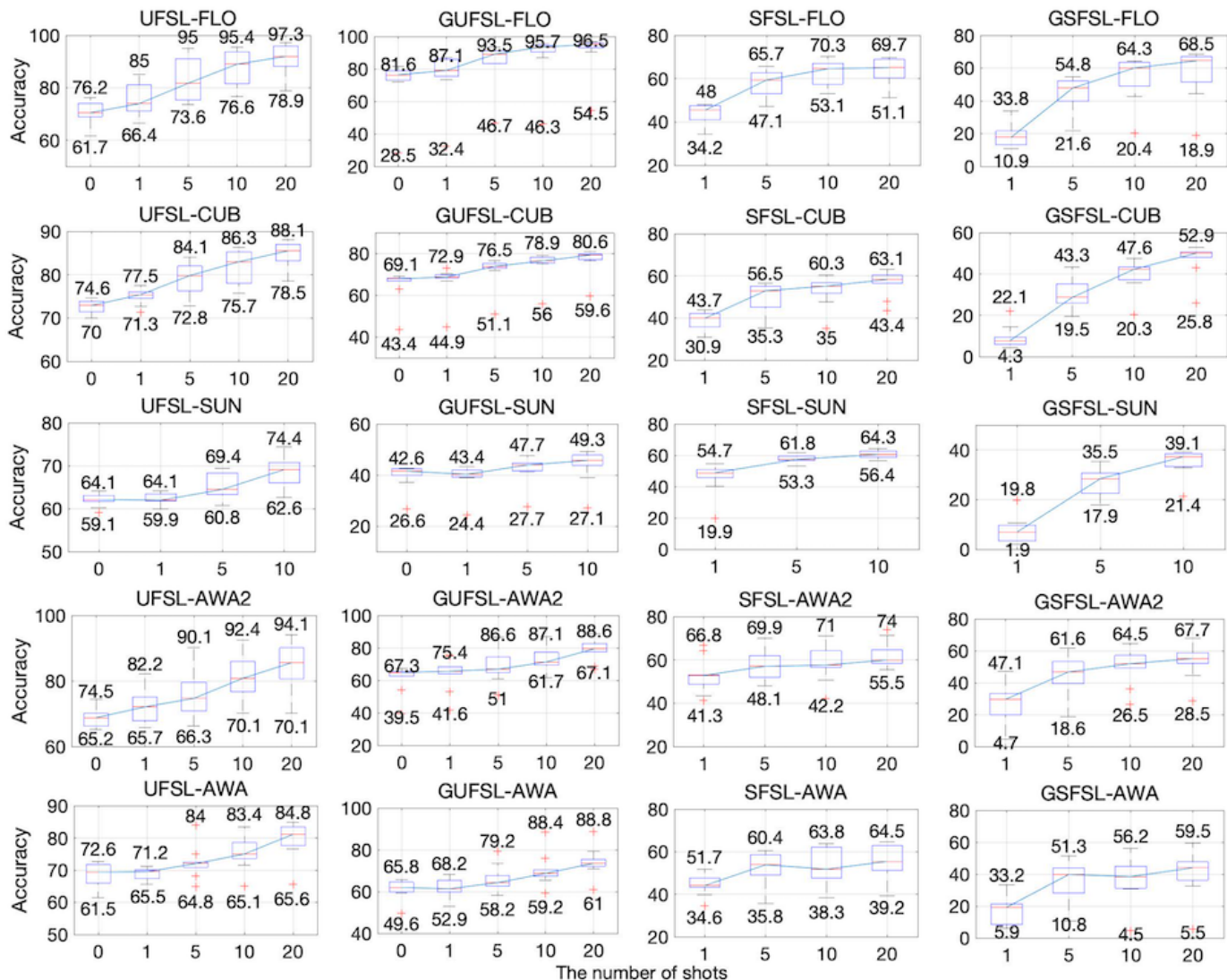


Fig. 6. Visualization of the performance of ten EAGMs for UFSL, GUFSL, SFSL, and GSFSL on the five benchmark datasets.

#Rank	Rank											Ave.
	1	2	3	4	5	6	7	8	9	10	--	
F-CLS												7.8
Lis												5.9
Lsr												3.4
CVAE												7.2
CADA												1.8
VAE-c												3.4
F-VAE												6.0
H-VAE												4.7
FREE												6.7
GCM												6.7

(a) UFSL

#Rank	Rank											Ave.
	1	2	3	4	5	6	7	8	9	10	--	
F-CLS												6.6
Lis												4.1
Lsr												2.9
CVAE												9.4
CADA												1.6
VAE-c												5.7
F-VAE												6.1
H-VAE												3.8
FREE												5.8
GCM												1.74

(b) GUFSL

#Rank	Rank											Ave.
	1	2	3	4	5	6	7	8	9	10	--	
F-CLS												6.5
Lis												5.6
Lsr												5.9
CVAE												8.6
CADA												4.2
VAE-c												4.0
F-VAE												4.8
H-VAE												3.5
FREE												5.1
GCM												5.6

(c) SFSL

#Rank	Rank											Ave.
	1	2	3	4	5	6	7	8	9	10	--	
F-CLS												6.6
Lis												4.4
Lsr												6.3
CVAE												7.8
CADA												2.1
VAE-c												6.7
F-VAE												4.5
H-VAE												3.5
FREE												5.5
GCM												6.1

(d) GSFSL

Fig. 7. Ranks of ten EAGMs for FSL. For each model, the ranks of the twenty results (five dataset  $\times$  four scenarios of different shots) of each task are shown, and "-" denotes the result is missing.

all the datasets, since the one-shot perseen sample scenario produces a weak baseline.

Third, we visualize the performance of ten EAGMs for UFSL, GUFSL, SFSL, and GSFSL on the five benchmark datasets in Figure 6. As shown, the performance of EAGMs deteriorates in order for the four tasks. In other words, the difficulty of the four tasks increases in turn. For example, the best performance of UFSL and GUFSL is about 85%  $\sim$  98% and 80%  $\sim$  97%, respectively. And the best performance of SFSL and GSFSL is about 60%  $\sim$  75% and 40%  $\sim$  70%, respectively. More models and techniques can be designed to address SFSL and GSFSL. The results shown in Figure 6 also demonstrate that increasing the number of samples in FSL could generally improve the performance of EAGMs. In addition, we can find that there are some outliers in the visualization of the results of GUFSL in Figure 6, which show degraded performance in comparison with others. These outliers are caused by CVAE, which is a naive generator and does not take the classification ability and visual-semantic matching into consideration.

Fourth, we present the ranks of different models for UFSL, GUFSL, SFSL, and GSFSL in Figure 7. For UFSL, CADA-VAE, LsrGAN, and VAE-cFlow usually present su-

rior performance than other models, whose average ranks are 1.8, 3.4, and 3.4. For GUFSL, CADA-VAE and LsrGAN also obtain satisfactory performance, whose average ranks are 1.6 and 2.9, respectively. For SFSL, the best models are VAE-cFlow and tf-VAEGAN, whose average ranks are 4.0 and 3.5, respectively. For GSFSL, the best models are CADA-VAE and tf-VAEGAN, whose average ranks are 2.1 and 3.5, respectively. As listed in Table 3, all of LsrGAN, CADA-VAE, tf-VAEGAN have a regularization on visual-semantic matching, which may contribute to the performance for few-shot learning.

Finally, we use the designed imbalanced GRU-based descriptions of FLO for few-shot learning. The results are summarized in Table 13. Through comparing the results in Table 13 and the results in Table 12, we can find that the designed imbalanced GRU-based descriptions indeed improve the performance of EAGMs for few-shot learning. Generally, an accuracy improvement of 3% ~ 6% for few-shot learning and generalized few-shot learning can be observed.

## 7 CONCLUSIONS

In this paper, we comprehensively evaluate a significant number of state-of-the-art EAGMs, *i.e.*, f-CLSWGAN, LisGAN, LsrGAN, CVAE, CADA-VAE, VAE-cFlow, f-VAEGAN-D2, tf-VAEGAN, FREE, and GCM, on five benchmark datasets, *i.e.*, FLO, CUB, SUN, AWA2, and AWA, within a unified evaluation protocol for ZSL, GZSL, UFSL, GUFSL, SFSL, and GSFSL. Four types of visual embeddings, *i.e.*, the original features, naive features, finetuned features, and regularized features, and four types of semantic embeddings, *i.e.*, the original descriptions, naive descriptions, GRU-based descriptions, and imbalanced GRU-based descriptions, are designed and provided to explore the effects of embeddings on EAGMs in depth.

First, our evaluation shows that accuracy improvement for ZSL and GZSL could be obtained from both the visual and semantic embeddings. On the one hand, introducing the visual information and semantic information of seen classes into the visual embedding of EAGMs could improve model performance on both the seen and unseen classes. For examples, the regularized features present an average  $Z$  improvement of 6.2% and 13.5% on FLO and CUB, respectively, and present an average  $H$  improvement of 8.7% and 13.6% on FLO and CUB, respectively. The results demonstrate that the category knowledge could indeed be transferred from the seen to unseen classes by the embedding-aware generative paradigm. On the other hand, modifying the current semantic embedding could also boost EAGMs easily, *e.g.*, applying GRU to release the overfitting of LSTM on seen classes and giving more weights to the loss of semantic features in model training. For FLO, the introduced imbalanced GRU-based descriptions present an average  $Z$  improvement of 3.4% in the ZSL setting and present an average  $H$  improvement of 2.3% in the GZSL setting. The significant improvements reveal the importance of embeddings to EAGMs. The researches on EAGM-based ZSL and GZSL should not be limited to the generator. The visual embedding and semantic embedding of EAGMs deserve more attentions.

TABLE 13  
Results of FSL with Imbalanced GRU-based Descriptions on FLO

Type	Method	Task	Shots	FLO						
				$Z$	$ZT$	$U$	$S$	$H$	$HT$	
GAN-based methods	f-CLSWGAN (2018)	(G)UFSL	1	77.2		72.8	93.8	82.0		
			5	87.1	1.08	87.0	96.5	91.5		
			10	95.0		94.4	97.4	95.9	1.37	
		20	95.8		95.8	97.4	96.6			
		1	<b>50.9</b>		36.5	20.9	13.4			
		5	65.8		53.0	53.4	53.2			
	(G)SFSL	10	66.9	0.19	61.6	62.9	62.2		26.5	
		20	68.7		61.2	74.1	67.0			
		1	-		-	-	-			
	LisGAN (2019)	(G)UFSL	5	86.4	1.45	86.0	97.8	91.5		
			10	89.5		91.5	97.7	94.5		1.66
			20	92.5		94.3	97.2	95.7		
1		-		-	-	-				
(G)SFSL		5	<b>65.9</b>		59.0	52.3	55.5			
		10	<b>69.0</b>	1.43	61.8	<b>68.3</b>	<b>64.9</b>		1.29	
	20	68.2		60.4	76.7	67.6				
LsrGAN (2020)	(G)UFSL	1	84.8		<b>82.0</b>	94.8	<b>88.0</b>			
		5	<b>92.6</b>	1.66	89.3	96.4	92.7		1.73	
		10	95.6		93.3	<b>98.2</b>	95.7			
	20	<b>98.2</b>		<b>96.6</b>	97.8	<b>97.2</b>				
	1	47.4		34.0	28.5	31.0				
	5	63.7		52.5	60.7	<b>56.3</b>				
(G)SFSL	10	67.6	0.24	<b>64.0</b>	63.4	63.7		0.74		
	20	69.0		63.3	72.4	67.5				
	1	74.5		32.1	<b>98.0</b>	48.4				
CVAE (2017)	(G)UFSL	5	84.6	0.05	51.4	<b>98.2</b>	67.5			
		10	88.3		64.2	98.0	77.6		0.78	
		20	90.5		73.2	<b>97.9</b>	83.7			
	1	35.0		14.2	<b>43.1</b>	21.4				
	(G)SFSL	5	54.4		16.3	64.1	26.0			
		10	53.1	0.09	17.4	67.3	27.7		2.21	
20		54.1		13.7	70.2	23.0				
CADA-VAE (2019)	(G)UFSL	1	<b>85.9</b>		76.7	96.8	85.6			
		5	91.4	<b>0.05</b>	89.6	96.9	93.1		<b>0.06</b>	
		10	94.2		92.0	97.1	94.5			
	20	95.1		94.1	96.4	95.2				
	1	40.5		33.5	38.6	<b>35.9</b>				
	5	58.3	<b>0.01</b>	46.7	<b>66.2</b>	54.7		<b>0.01</b>		
VAE-cFlow (2020)	(G)UFSL	10	61.8		53.2	65.4	58.7			
		20	62.0		47.5	<b>77.5</b>	58.9			
		1	77.6		69.7	93.2	79.7			
	5	89.5		85.6	94.4	89.8				
	10	92.4	0.47	90.1	94.7	92.3		0.47		
	20	94.2		94.1	94.2	94.1				
f-VAEGAN-D2 (2019)	(G)UFSL	1	45.6		31.5	5.5	9.4			
		5	57.8		56.5	28.2	37.6			
		10	60.2	0.45	54.5	44.8	49.1		0.45	
	20	62.5		55.2	51.7	53.4				
	1	76.7		75.2	92.5	83.0				
	5	78.1	2.85	76.5	95.8	85.1		3.89		
10	85.8		86.3	96.4	91.0					
20	92.7		93.1	96.8	94.9					
tf-VAEGAN (2020)	(G)SFSL	1	50.0		22.2	11.9	15.5			
		5	62.5		58.0	38.7	46.4			
		10	67.6	1.80	58.6	66.7	62.4		1.39	
	20	67.5		<b>65.5</b>	72.4	68.8				
	1	82.4		80.0	95.9	87.2				
	5	92.1	8.97	<b>90.7</b>	97.3	<b>93.9</b>		8.58		
10	<b>95.4</b>		<b>95.0</b>	97.4	<b>96.2</b>					
20	96.2		96.2	97.2	96.7					
FREE (2021)	(G)UFSL	1	48.9		<b>42.2</b>	19.1	26.3			
		5	64.0		58.4	52.5	55.3			
		10	67.0	1.23	61.6	67.6	64.5		1.83	
	20	68.7		64.1	74.4	<b>68.9</b>				
	1	76.8		74.5	93.1	82.8				
	5	82.3		85.9	97.4	91.3				
10	90.2	6.36	92.5	97.3	94.8		7.25			
20	96.3		95.8	97.1	96.5					
GCM-CF (2021)	(G)SFSL	1	48.9		15.6	20.5	17.7			
		5	63.1		<b>59.9</b>	45.2	51.5			
		10	67.0	6.31	62.2	62.4	62.3		6.49	
	20	<b>69.1</b>		64.9	72.9	68.7				
	1	74.9		73.9	90.6	81.4				
	5	83.2		84.0	91.7	87.7				
10	86.7	2.89	88.4	92.1	90.2		2.91			
20	91.5		92.9	92.8	92.8					
(G)SFSL	1	41.8		18.5	10.3	13.2				
	5	54.7	0.54	42.5	44.2	43.3				
	10	60.6		41.0	55.4	47.1				
	20	62.5		39.8	59.9	47.8				

Note: RED FONT and BLUE FONT denote the best results for (G)UFSL and (G)SFSL, respectively

Second, considering that there is actually no agreed upon protocols for the fair comparison of EAGM-based FSL, we reproduce ten EAGMs and utilize the modified embeddings to give a strong baseline for UFSL, GUFSL, SFSL and GSFSL on five benchmark datasets. The results of one-shot, five-



shot, ten-shot, and twenty-shot scenarios are presented for each task. On the one hand, our experiments show that the performance of EAGMs in FSL could be improved with the increasing of the number of samples. For example, in the UFSL setting, the average  $Z$  of ten EAGMs on five datasets of one-shot, five-shot, ten-shot, and twenty-shot learning is 71.2%, 75.7%, 79.2%, and 85.2%. And in the GUFSL setting, the average  $H$  of one-shot, five-shot, ten-shot, and twenty-shot learning is 62.4%, 67.4%, 70.9%, and 81.1%. The improvements by the increasing of the number of samples demonstrate the effectiveness of EAGMs for few-shot learning. On the other hand, our experimental results reveal that the challenge of UFSL, GUFSL, SFSL and GSFSL for EAGMs increases in turn. For example, the highest accuracy of the four tasks on FLO is 97.3%, 96.6%, 71.1%, and 69.2%, and the highest accuracy on CUB is 88.1%, 80.6%, 63.1%, and 52.9%. Especially, in experiments, SFSL and GSFSL show extremely challenging for current EAGMs, since there are only a few seen samples used for model training. The low dependence on samples makes SFSL and GSFSL more practical in the real world and have more potential for future learning.

Finally, we summarize our works, including the four kinds of semantic and visual features, ten generative models, optimized parameters, and data splits for six tasks, in the publicly available GASL repository to foster the researches on EAGMs. With GASL, the state-of-the-art results of ZSL, GZSL, UFSL, GUFSL, SFSL, and GSFSL can be readily reproduced for various data insufficiency scenarios, and hence new methods, regularizations, and features can be sufficiently and fairly evaluated.

## ACKNOWLEDGMENTS

This work is supported by the National Science Fund for Distinguished Young Scholars (No. 62125306), the Fundamental Research Funds for the Central Universities (Zhejiang University NGICS Platform), and the Research Project of the State Key Laboratory of Industrial Control Technology (ICT2021A15).

## REFERENCES

- [1] D. Jia, D. Wei, R. Socher, *et al.* "ImageNet: a large-scale hierarchical image database." in *Proc. IEEE Conf. CVPR*, 2009, pp. 248-255.
- [2] T. Y. Lin, M. Maire, S. Belongie, *et al.* "Microsoft COCO: common objects in context." *Springer International Publishing*, 2014.
- [3] Y. Lecun, Y. Bengio, G. Hinton. "Deep learning." *Nature*, vol. 521, no. 7553, pp. 436, 2015.
- [4] L. J. Feng, C. H. Zhao, *et al.* "BNGBS: An efficient network boosting system with triple incremental learning capabilities for more nodes, samples, and classes," *Neuro.*, vol. 412, no. 28, pp. 486-501, 2020
- [5] C. Szegedy, *et al.* "Rethinking the inception architecture for computer vision." in *Proc. IEEE Conf. CVPR*, 2016, pp. 2818-2826.
- [6] K. Simonyan, A. Zisserman. "Very deep convolutional networks for large-scale image recognition." in *Proc. ICLR*, 2015.
- [7] A. Vaswani, N. Shazeer, *et al.* "Attention is all you need." in *Proc. Conf. NIPS*, 2017, pp. 6000-6010.
- [8] A. Dosovitskiy, L. Beyer, A. Kolesnikov, *et al.* "An Image is worth 16x16 words: Transformers for image recognition at scale." <https://arxiv.org/abs/2010.11929>, 2020.
- [9] L. Yuan, Y. Chen, *et al.* "Tokens-to-token ViT: training vision transformers from scratch on ImageNet." <http://arxiv.org/abs/2101.11986>, 2021.
- [10] L. J. Feng, *et al.* , "Dual Attention-Based Encoder-Decoder: A Customized Sequence-to-Sequence Learning for Soft Sensor Development," *IEEE TNNLS*, vol. 32, no. 8, pp. 3306-3317, 2020.
- [11] T. H. Chan, K. Jia, *et al.* "PCANet: A simple deep learning baseline for image classification?." *IEEE Trans. Image Process.*, vol. 24, no. 12, pp. 5017-5032, 2015.
- [12] W. K. Yu, C. H. Zhao. "Low-rank characteristic and temporal correlation analytics for incipient industrial fault detection with missing data," *IEEE TII*, DOI: 10.1109/TII.2020.2990975, 2021.
- [13] K. He, *et al.* "Deep residual learning for image recognition." in *Proc. IEEE Conf. CVPR*, Jun. 2015, pp. 770-778.
- [14] W. K. Yu, C. H. Zhao, "Broad Convolutional Neural Network based Industrial Process Fault Diagnosis with Incremental Learning Capability," *IEEE TIE*, vol. 67, no. 6, pp. 5081-5091, 2020.
- [15] C. H. Lampert, H. Nickisch, and S. Harmeling. "Learning to detect unseen object classes by between-class attribute transfer." in *Proc. IEEE Conf. CVPR*, 2009, pp. 951-958.
- [16] P. Feng, P. J. Pan, *et al.* "Zero shot on the cold-start problem: model-agnostic interest learning for recommender systems," in *ACM CIKM*, <https://arxiv.org/abs/2108.13592>, 2021.
- [17] L. J. Feng, C. H. Zhao. "Fault description based attribute transfer for zero-sample industrial fault diagnosis," *IEEE Trans. Ind. Inf.*, vol. 17, no. 3, pp. 1852-1862, 2021.
- [18] B. Romera-Paredes and P. H. S. Torr. "An embarrassingly simple approach to zero-shot learning", in *Proc. ICML*, 2015, pp. 2152-2161.
- [19] S. Changpinyo, W. Chao, *et al.* "Synthesized classifiers for zero-shot learning." in *Proc. IEEE Conf. CVPR*, 2016, pp. 5327-5336.
- [20] Y. Hu, *et al.* "Semantic graph-enhanced visual network for zero-shot learning." <https://arxiv.org/pdf/2006.04648.pdf>, 2020.
- [21] F. Ali, *et al.* "Describing objects by their attributes." in *Proc. IEEE Conf. CVPR*, 2009, pp. 1778-1785.
- [22] R. B. Xie, Z. Y. Liu, *et al.* "Representation learning of knowledge graphs with entity descriptions." in *Proc. AAAI*, 2016.
- [23] Z. Akata, F. Perronnin, *et al.* "Label-embedding for attribute-based classification." in *Proc. IEEE Conf. CVPR*, 2013, pp. 819-826.
- [24] F. Zhang and G. Shi. "Co-representation network for generalized zero-shot learning." in *Proc. ICML*, 2019.
- [25] S. Reed, Z. Akata, *et al.* "Learning deep representations of fine-grained visual descriptions." in *Proc. IEEE Conf. CVPR*, 2016, 49-58.
- [26] M. E. Nilsback and A. Zisserman. "Automated flower classification over a large number of classes." in *Proc. ICCVGI*, 2008.
- [27] Y. Xian, *et al.* "Zero-shot learning - the good, the bad and the ugly." in *Proc. IEEE Conf. CVPR*, 2017, pp. 3077-3086.
- [28] Y. Xian, C. H. Lampert, *et al.* "Zero-shot learning - a comprehensive evaluation of the good, the bad and the ugly." *IEEE Trans. Pattern Anal. Mach. Intell.*, vol. 41, no. 9, pp. 2251-2265, 2019.
- [29] S. Deutsch, *et al.* , "Zero-shot learning via multi-scale manifold regularization." in *Proc. IEEE Conf. CVPR*, 2017, pp. 292-5299.
- [30] S. B. Min, *et al.* "Domain-aware visual bias eliminating for generalized zero-shot learning," in *Proc. CVPR*, 2020, pp. 12661-12670.
- [31] Z. Fu, T. A. Xiang, *et al.* "Zero-shot object recognition by semantic manifold distance," in *Proc. IEEE Conf. CVPR*, 2015, pp. 2635-2644.
- [32] D. Huynh, E. Elhamifar. "Fine-grained generalized zero-shot learning via dense attribute-based attention," in *Proc. IEEE Conf. CVPR*, 2020.
- [33] B. Liu, Q. Dong, Z. Hu. "Zero-shot learning from adversarial feature residual to compact visual feature." in *Proc. AAAI*, 2020.
- [34] Ye, M., Y. Guo. "Progressive ensemble networks for zero-shot recognition." in *Proc. IEEE Conf. CVPR*, 2019, pp. 11728-11736.
- [35] Y. L. Yu, Z. Ji, *et al.* "Episode-based prototype generating network for zero-shot learning," in *Proc. IEEE Conf. CVPR*, 2020.
- [36] W. L. Chao, S. Changpinyo, *et al.* "An empirical study and analysis of generalized zero-shot learning for object recognition in the wild." in *Proc. IEEE Conf. CVPR*, 2016, pp. 52-68.
- [37] J. Shao, X. Li. "Generalized zero-shot learning with multi-channel Gaussian mixture VAE," *IEEE Signal Process. Let.*, vol. 27, pp. 456-460. 2020.
- [38] L. J. Feng, C. H. Zhao. "Transfer increment for generalized zero-shot learning." in *IEEE Trans. Neural Net. and Learn. syst.*, 2020.
- [39] H. Zhang, Y. Long, *et al.* "Triple verification network for generalized zero-shot learning," *IEEE Trans. Image Process.*, vol. 28, no. 1, pp. 506-517, 2019.
- [40] Z. Ji, Y. Sun, Y. Yu, *et al.* "Attribute-guided network for cross-modal zero-shot hashing," *IEEE Trans. Neural Netw. Learn. Syst.*, vol. 31, no. 1, pp. 321-330, 2020.

- [41] A. Frome, G. S. Corrado, J. Shlens, S. Bengio, J. Dean, M. A. Ranzato, and T. Mikolov, "Devise: a deep visual-semantic embedding model," in *Proc. Advances Neural Inf. Process. Syst.*, 2013, pp. 2121–2129.
- [42] X. Wang, *et al.*, "Zero-shot recognition via semantic embeddings and knowledge graphs." in *Proc. CVPR*, 2018, pp. 1211–1219.
- [43] E. Christian, W. Anton, and L. Rainer. "On the benefit of synthetic data for company logo detection." in *ACM Multimedia*, 2015.
- [44] A. Radford, L. Metz, and S. Chintala. "Unsupervised representation learning with deep convolutional generative adversarial networks," in *ICLR*, 2016.
- [45] X. Wang and A. Gupta. "Generative image modeling using style and structure adversarial networks." In *ECCV*, 2016.
- [46] Y. Li, K. Swersky, *et al.* "Generative moment matching networks." in *Proc. IEEE Conf. CVPR*, 2015, pp.1718–1727.
- [47] A. Odena, C. Olah, *et al.* "Conditional image synthesis with auxiliary classifier gans." in *Proc. ICML*, 2017.
- [48] Y. Xian, T. Lorenz, *et al.* "Feature generating networks for zero-shot learning," in *Proc. IEEE Conf. CVPR*, 2018, pp. 5542–5551.
- [49] M. Bucher, S. Herbin, and F. Jurie. "Generating visual representations for zero-shot classification." arXiv preprint arXiv:1708.06975, 2017.
- [50] V. K. Verma, G. Arora, A. Mishra, and P. Rai, "Generalized zero-shot learning via synthesized examples," in *Proc. IEEE Conf. CVPR*, Jun. 2018, pp. 4281–4289.
- [51] C. Xie, H. Xiang, T. Zeng, Y. Yang, B. Yu, and Q. Liu. "Cross knowledge-based generative zero-shot learning approach with taxonomy regularization," *Neural Networks*, vol. 139, pp. 168–178, 2021.
- [52] M. B. Sariyildiz, R. G. Cinbis, *et al.* "Gradient matching generative networks for zero-shot learning," in *Proc. IEEE Conf. CVPR*, 2019, pp. 2163–2173.
- [53] H. Huang, *et al.* "Generative dual adversarial network for generalized zero-shot learning." <https://arxiv.org/abs/1811.04857v1>, 2018.
- [54] D. Wang, Y. Li, *et al.* "Relational knowledge transfer for zero-shot learning," in *Proc. AAAI*, Mar. 2016, pp. 1–7.
- [55] B. Zhao, B. Wu, *et al.* Zero-shot learning posed as a missing data problem. in *Proc. IEEE Conf. CVPR*, 2017, pp. 2616–2622.
- [56] M. Arjovsky, S. Chintala, and L. Bottou. "Wasserstein GAN." in *Proc. ICML*, 2017.
- [57] I. J. Goodfellow, J. P. Abadie, *et al.* "Generative adversarial networks." in *Proc. NIPS*, 2014, pp. 2672–2680.
- [58] E. Bodin, I. Malik, *et al.* "Nonparametric inference for auto-encoding variational Bayes." <https://arxiv.org/abs/1712.06536>, 2017.
- [59] D. P. Kingma, M. Welling. "Auto-encoding variational Bayes." <https://arxiv.org/abs/1312.6114>, 2013.
- [60] W. I. Wang, Y. C. Pu, *et al.* "Zero-shot learning via class conditioned deep generative models." in *Proc. AAAI*, 2018.
- [61] R. Gao, X. Hou, *et al.* "Zero-vae-gan: Generating unseen features for generalized and transductive zero-shot learning." *IEEE Trans. Image Process.*, vol. 29, pp. 3665–3680, 2020.
- [62] Z. Y. Han, Z. Y. Fu, J. Yan, "Learning the redundancy-free features for generalized zero-shot object recognition," in *Proc. IEEE Conf. CVPR*, 2020, pp. 12862–12871.
- [63] Y. Zhu, M. Elhoseiny, *et al.* "A generative adversarial approach for zero-shot learning from noisy texts." in *Proc. IEEE Conf. CVPR*, 2018, pp. 1004–1013.
- [64] Y. Bengio, L. Yao, *et al.* "Generalized denoising auto-encoders as generative models." in *Proc. NIPS*, 2013.
- [65] R. Felix, B. G. V. Kumar, *et al.* "Multimodal cycle-consistent generalized zero-shot learning," in *Proc. ECCV*, 2018.
- [66] Y. L. Yu, Z. Ji, *et al.* "Episode-based prototype generating network for zero-shot learning," in *Proc. IEEE Conf. CVPR*, 2020, pp. 14035–14044.
- [67] Y. Xian, S. Sharma, *et al.* "f-VAEGAN-D2: a feature generating framework for any-shot learning", in *Proc. IEEE Conf. CVPR*, 2019, pp. 10267–10276.
- [68] S. M. Chen, W. J. Wang, *et al.* "FREE: Feature refinement for generalized zero-shot learning", in *Proc. IEEE Conf. ICCV*, 2021.
- [69] S. Rahman, S. Khan, and F. Porikli. "A unified approach for conventional zero-shot, generalized zero-shot and few-shot learning." *IEEE Trans. Image Process.*, vol. 27, no. 11, pp. 5652–5667, 2018.
- [70] S. Jake, S. Kevin, *et al.* "Prototypical networks for few-shot learning," in *Proc. NIPS*, 2017, pp. 4080–4090.
- [71] S. Blaes, T. Burwick. "Few-shot learning in deep networks through global prototyping." *Neural networks*, vol. 94, pp. 159–172, 2017.
- [72] F. Sung, Y. Yang, L. Zhang, *et al.* "Learning to compare: relation network for few-shot learning." in *Proc. IEEE Conf. CVPR*, 2018.
- [73] C. Finn, P. Abbeel, and S. Levine. "Model-agnostic meta-learning for fast adaptation of deep networks." in *Proc. ICML*, 2017, pp. 1126–1135.
- [74] O. Vinyals, C. Blundell, *et al.* "Matching networks for one shot learning." in *Proc. NIPS*, 2016, pp. 3637–3645.
- [75] M. Rohrbach, S. Ebert, and B. Schiele. "Transfer learning in a transductive setting." in *Proc. NIPS*, 2013, pp. 46–54.
- [76] V. K. Verma, D. Brahma, P. Rai. "Meta-learning for generalized zero-shot learning," in *Proc. IEEE Conf. AAAI*, 2020, pp. 6062–6069.
- [77] F. Pahde, M. Puscas, T. Klein, *et al.* "Multimodal prototypical networks for few-shot learning," in *IEEE Winter Conference on Applications of Computer Vision (WACV)*. IEEE, 2021.
- [78] Z. Ji, X. Chai, Y. Yu, *et al.* "Improved prototypical networks for few-shot learning," *Pattern Recognition Letters*, pp.140, 2020.
- [79] E. Schonfeld, S. Ebrahimi, *et al.* "Generalized zero- and few-shot learning via aligned variational autoencoders." in *Proc. IEEE Conf. CVPR*, 2019, pp. 8247–8255.
- [80] C. Zhang, X. Lyu, Z. Tang. "TGG: transferable graph generation for zero-shot and few-shot learning," in *Proc. ACM Int. Conf. on Multimedia*, 2019, pp. 1641–1649.
- [81] F. Y. Song and Y. Chen. "A survey on zero-shot learning," *Journal of Science*, vol. 5, no. 1, pp. 455–460, 2016.
- [82] J. Y. Chen, Y. X. Geng, *et al.*, "Knowledge-aware zero-shot learning: survey and perspective," in *Proc. IJCAI*, 2021.
- [83] Y. W. Fu, T. Xiang, Y. G. Jiang, *et al.* "Recent advances in zero-shot recognition: toward data-efficient understanding of visual content," *IEEE Signal Processing Magazine*, vol. 35, no. 1, 112–125, 2018.
- [84] W. Wang, V. W. Zheng, H. Yu, *et al.* "A survey of zero-shot learning: settings, methods, and applications," *ACM Transactions on Intelligent Systems and Technology*, vol. 10, no. 2, pp. 1–37, 2019.
- [85] F. Pourpanah, M. Abdar, Y. Luo, *et al.* "A review of generalized zero-shot learning methods," <https://arxiv.org/abs/2011.08641>, 2020.
- [86] S. J. Pan, Y. Qiang. "A survey on transfer learning," *IEEE Transactions on Knowledge and Data Engineering*, vol. 22, no.10, pp.1345–1359, 2010.
- [87] K. Weiss, T. M. Khoshgoftaar, D. D. Wang. "A survey of transfer learning." *Journal of Big Data*, vol. 3, no.1, pp.1–40, 2016.
- [88] S. Ling, Z. Fan, X. Li. "Transfer learning for visual categorization: a survey." *IEEE Transactions on Neural Networks and Learning Systems*, vol. 26, no.5, pp.1019, 2014.
- [89] Y. Liu. "A review about transfer learning methods and applications." in *Proc. International Conference on Information and Network Technology*, 2011.
- [90] T. Yoshida, H. Ogino. "Theoretical analysis and evaluation of topic graph based transfer learning," in *Proc. International Conference on Active Media Technology*, Springer-Verlag New York, Inc. 2013.
- [91] Y. Wang, Q. Yao, J. Kwok, *et al.* "Generalizing from a few examples: a survey on few-shot learning," <https://arxiv.org/abs/1904.05046>, 2019.
- [92] S. Jia, S. Jiang, Z. Lin, *et al.* "A survey: deep learning for hyperspectral image classification with few labeled samples," *Neurocomputing*, vol. 448, no. 11, pp. 179–204, 2021.
- [93] T. Hospedales, A. Antoniou, P. Micaelli, *et al.* "Meta-learning in neural networks: a survey." *IEEE Trans. Pattern Analysis and Machine Learning*, 2020.
- [94] D. Mandal, S. Medya, B. Uzzi, *et al.* "Meta-learning with graph neural networks: methods and applications." <https://arxiv.org/abs/2103.00137v1>, 2021.
- [95] X. Li, L. Yu, C. W. Fu, *et al.* "Revisiting metric learning for few-shot image classification." *Neurocomputing*, vol. 406, no. 17, pp. 49–58, 2020.
- [96] Z. Ji, Y. Sun, Y. Yu, *et al.* "Attribute-guided network for cross-modal zero-shot hashing," *IEEE Trans. Neural Netw. Learn. Syst.*, vol. 31, no. 1, pp. 321–330, 2020.
- [97] Y. Liu, J. Guo, *et al.* "Attribute attention for semantic disambiguation in zero-shot learning," in *Proc. IEEE Conf. CVPR*, 2019, pp. 6697–6706.

- [98] R. Keshari, R. Singh, M. Vatsa. "Generalized zero-shot learning via over-complete distribution." in *Proc. IEEE Conf. CVPR*, 2020.
- [99] V. K. Verm and P. Rai. "A simple exponential family framework for zero-shot learning." in *Proc. ECML*, 2017, pp. 792-808.
- [100] Meng Ye and Yuhong Guo. "Zero-shot classification with discriminative semantic representation learning." in *Proc. IEEE Conf. CVPR*, 2017, pp. 5103-5111.
- [101] J. Song, C. Shen, *et al.* "Transductive unbiased embedding for zero-shot learning." in *Proc. IEEE Conf. CVPR*, 2018.
- [102] J. Li, M. Jin, *et al.* "Leveraging the invariant side of generative zero-shot learning," in *Proc. IEEE Conf. CVPR*, 2019, pp. 7394-7403.
- [103] M. R. Vyas, *et al.* , "Leveraging seen and unseen semantic relationships for generative zero-shot learning," in *Proc. ECCV*, 2020.
- [104] A. Mishra, M. Reddy, A. Mittal, *et al.* "A generative model for zero-shot learning using conditional variational autoencoders," in *Proc. IEEE Conf. CVPR*, 2017.
- [105] Y. C. Gu, L. Zhang, Y. Liu, *et al.* "Generalized zero-shot learning via VAE-conditioned generative flow." in *Proc. IEEE Conf. CVPR*, 2020.
- [106] F. Ye, A. G. Bors. "InfoVAEGAN: learning joint interpretable representations by information maximization and maximum likelihood," in *Proc. Int. Conf. on Image Processing (ICIP)*, pp. 749-753, 2021.
- [107] S. Narayan, A. Gupta, *et al.* "Latent embedding feedback and discriminative features for zero-shot classification," in *Proc. ECCV*, 2020.
- [108] Z. Q. Yue, T. Wang, *et al.* . "Counterfactual zero-shot and open-set visual recognition," in *Proc. IEEE Conf. CVPR*, pp. 15404-15414, 2021.
- [109] Y. M. Shen, J. Qin, L. Huang. "Invertible Zero-Shot Recognition Flows," in *Proc. IEEE Conf. ECCV*, 2020, pp. 3722-3740.
- [110] C. Wah, S. Branson, *et al.* "The caltech-ucsd birds-200-2011 dataset." 2011.
- [111] G. Patterson and J. Hays. "Sun attribute database: discovering, annotating, and recognizing scene attributes." in *Proc. IEEE Conf. CVPR*, 2012. pp. 2751-2758.
- [112] C. Szegedy, L. Wei, Y. Jia, *et al.* "Going deeper with convolutions," in *Proc IEEE Conf. CVPR*, 2015.
- [113] D. P. Kingma and J. Ba. "Adam: a method for stochastic optimization." arXiv preprint arXiv:1412.6980, 2014.
- [114] F. K. Gre, R. K. Srivastava, J. Koutník, *et al.* "LSTM: A Search Space Odyssey," *IEEE Transactions on Neural Networks & Learning Systems*, vol. 28, no. 10, pp.2222-2232, 2016.
- [115] B. Zhang, D. Xiong, J. Su. "A GRU-gated attention Model for neural machine translation," *IEEE Transactions on Neural Networks and Learning Systems*, 2017.
- [116] J. Donaldson. "T-sne: T-distributed stochastic neighbor embedding for R (t-SNE)." *J. Mach. Learn. Res.*, 2012.



**Jiancheng Zhao** received his B.Eng. from the Zhejiang University, Zhejiang, China, in 2021. Now, he is pursuing his Ph.D. with the College of Control Science and Engineering, Zhejiang University, Hangzhou, China. His current research interests include zero-shot and few-shot learning.



**Chunhui Zhao** (SM'15) received the B.Eng., M.S., and Ph.D. degrees in Control Science and Engineering from the Department of Automation, Northeastern University, Shenyang, China, in 2003, 2006, and 2009, respectively. She was a Postdoctoral Fellow (January 2009-January 2012) at the Hong Kong University of Science and Technology, and the University of California, Santa Barbara, Los Angeles, CA, USA.

Chunhui Zhao is currently a full professor with the College of Control Science and Engineering, Zhejiang University, Hangzhou, China, since Jan. 2012. She has published over 170 papers in peer-reviewed international journals. Her research interests include machine learning and data mining. Prof. Zhao was a recipient of the National Science Fund for Distinguished Young Scholars, and New Century Excellent Talents in University, respectively.



**Liangjun Feng** received his B.Eng. from the North China Electric Power University, Beijing, China, in 2017. Now, he is pursuing his Ph.D. with the College of Control Science and Engineering, Zhejiang University, Hangzhou, China. He has authored or coauthored more than 10 papers in peer-reviewed international journals. He is the reviewer of several journals, including IEEE TIP, IEEE TNNLS, and IEEE TII. His current research interests include zero-shot and few-shot learning.